Heavy Fuel Engine

Prepared by:

Michigan Technological University

Mechanical Engineering, Engineering Mechanics Department

Scott Miers, Associate Professor

Brian Eggart, Research Engineer

Kyle Price, Andy Sleder

Contact Email: samiers@mtu.edu

Contact Phone: (906) 487-2709

In support of:

Contract Number W56HZV-14-C-0286

Work Directive 016, “Auxiliary Power Unit,” “Heavy Fuel Engine” DATE: 05/09/2019

For and with support by:

United States Department of the Army

Tank, Automotive, Research, and Development Engineering Center Ground Vehicle Power and Mobility

Non-primary Power Systems Team

Andrew Wiegand

Contact Email: andrew.l.wiegand.civ@mail.mil

Contact Phone: (586) 282-1770

Table of Contents

List of Figures

List of Tables

Project Goal and Objectives

The goal of this project was to demonstrate a power density increase on a commercial engine while operating on heavy fuels. The first objective was to build a dedicated, small-engine test cell to permit evaluation of a two-cylinder diesel engine under increased manifold pressure (boost) conditions and transfer lessons learned to the TARDEC Compact Military Power dynamometer system. The second objective was to establish a baseline set of parameters including power output, fuel consumption, exhaust gas temperature, heat rejection, smoke, combustion behavior by collecting data over a wide range of engine speeds and loads on a commercial off the shelf engine. The third objective was to study the impact on those baselined parameters through an increase in fueling for the naturally-aspirated engine. The fourth objective was to address high exhaust gas temperature due to extra fueling by modifying the fuel injection timing. The fifth objective was to evaluate F24 fuel compared to off-road diesel. The sixth objective was to study the impact of intake air pressure boosting on the above mentioned parameters.

Experimental Setup

Engine Test Cell Overview

The test cell for conducting this research consisted of a 150 kW eddy current dynamometer, two-cylinder diesel engine, data acquisition system, fuel supply system, and smoke meter. Engine cooling was accomplished using a liquid-to-liquid plate heat exchanger and engine boost was supplied by three air compressors installed in parallel to provide the necessary air during engine operation. Figure 1 shows the completed test cell and additional test cell hardware and software details are provided in Table 1.

Table 1: Test cell hardware and software

Instrument	Make	Model # / Part #
150 kW eddy current dynamometer	Froude-Hoffman	AG150HS (Purchased 12/2014)
Two cylinder indirect injection liquid cooled diesel engine	Kohler	KDW702
Engine heat exchanger	Bell and Gossett	BP400-20
Dyno heat exchanger	Bell and Gossett	BPW-70-12X5
Engine coolant flow controller	Belimo	B213+TRFB24-SR-NO (Cv of 4.7)
Dyno coolant flow controller	Belimo	B232+ARX24-SR-T (Cv of 37)
Dyno coolant pump	Gould	1ST1G4A4 (2 hp, 6.125” dia)
Driveshaft	MSI	Serial #: 654926-58
Dynamometer controller and data acquisition system	Land-and-Sea	DYNO-MAX 2010 Pro+
Combustion analyzer	AVL	IndiModul with IndiCom software
Smoke meter	AVL	415S
Fuel supply system	ReSol	RS485
Load control system	Land-and-Sea	430-312
Intake air heater	Cummins	3929108
Oil pan heater	Kat’s	24100
Engine isolator	GM	10284134

Figure 1: Test cell showing dynamometer, driveline, engine, and data acquisition system

Engine Test Cell Details

Dynamometer

The dynamometer was a 150kW, liquid-cooled, eddy-current with inertia of 0.092 kg-m^2. It was a single-ended dynamometer, with a custom starter installed on the opposite end. The total inertia of the dynamometer and ring gear was 0.121 kg-m^2. For this experiment, the engine starter was utilized for all engine start situations. Remote start was controlled from the operator's station. Dynamometer control was performed by DynoMax 2010 Pro software, a Land-and-Sea product. A screen capture of the dynamometer and data acquisition system is shown in Figure 2.

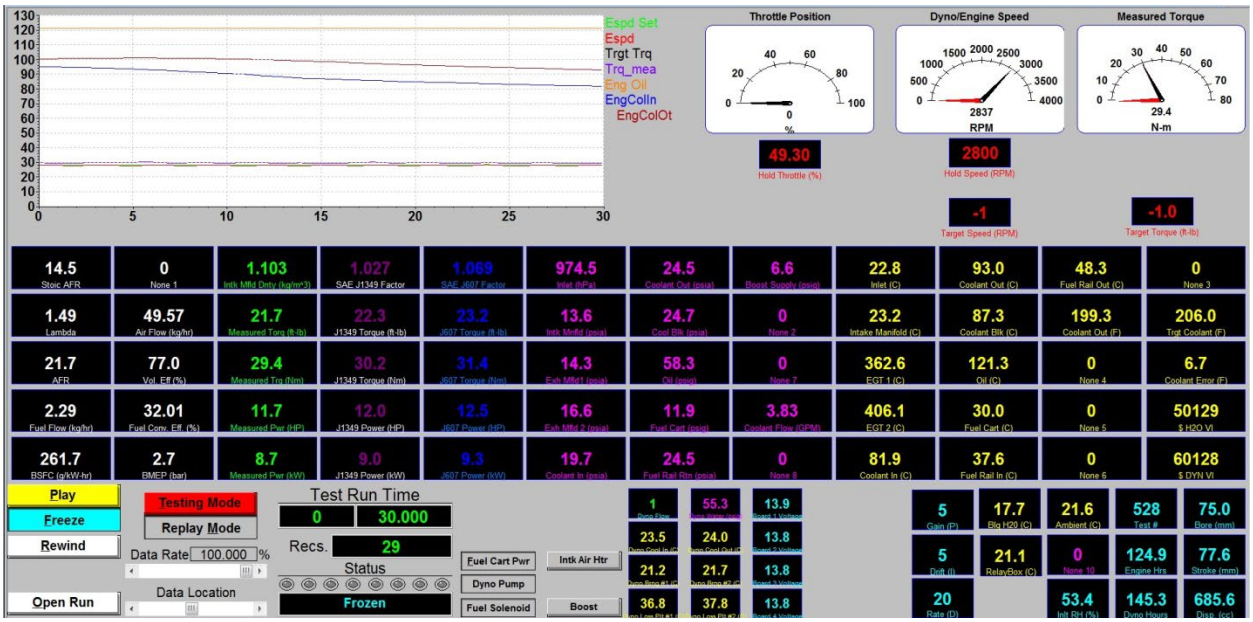

Figure 2: Dynamometer data acquisition and control system screen capture

Engine

The engine utilized for this testing was a two-cylinder, liquid-cooled, compression-ignition, indirect-injection, Kohler KDW702. Of worthwhile note is that while this engine is sold by Kohler, the original engine design is from Lombardini, an Italian engine manufacturer. Full engine specifications are shown in Table 2. The engine was purchased from Superior Diesel in Rhinelander, WI. The intake manifold was replaced from an integral air filter style (Kohler PN 8741_183) to a remote air filter style manifold (Kohler PN 2486_265).

Table 2: Engine specifications

Specification Number	PA-KDW702-1101A
Serial Number	4435200200
Bore (mm)	75
Stroke (mm)	77.6
Displacement (cc)	686
Compression Ratio	22.8:1
Cooling	Liquid
Fuel Delivery	Indirect Injection (Bosch Mechanical Injector)
Peak Power (kW)	11.5
Peak Torque (Nm)	34
Mass - dry (kg)	66
Power Density (kW/kg)	0.174

Driveline

The driveline was sized using the dynamometer inertia and an estimation of the engine inertia which included the flywheel and driveshaft adaptor (0.0687 kg-m^2). For this particular application, a driveshaft from Machine Service Incorporated (MSI) of Green Bay, WI was

purchased, with a torsional stiffness of 647 Nm/rad. The dynamometer side of the shaft was a SAE1410 and the engine side was a SAE1310. The shaft serial number was 654926-58. A picture of the shaft is shown in Figure 3.

Figure 3: MSI driveshaft

A driveline magnification factor analysis was performed using a simple 2-mass/spring system. The results of the analysis are shown in Figure 4. From the analysis, a resonance occurs around 1st order 1200 RPM. This was confirmed when operating between 800 and 1600 RPM resulted in damage to one of the first shafts tested on the engine due to failed rubber elements in the shaft.

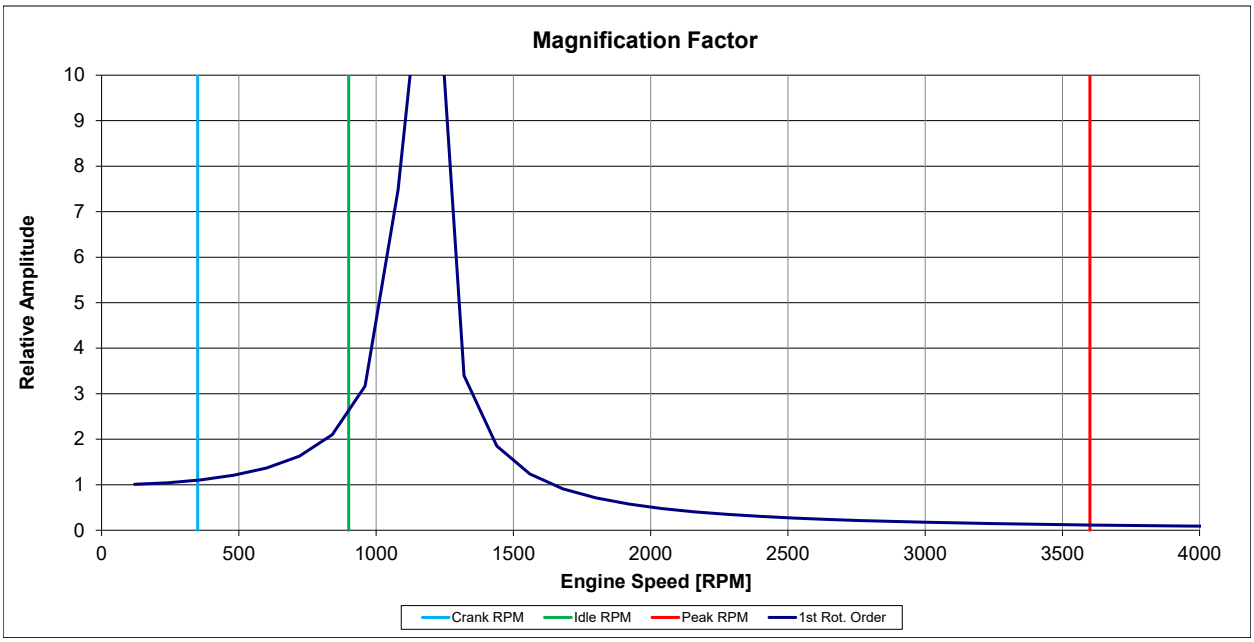

Figure 4: Driveline magnification factor

Emergency Shut-down System

A hard-wired Emergency-stop (E-stop) system was incorporated into the test cell that was used to quickly and safely shut down the test cell in the event of an emergency. The E-stop loop was powered by a 24 VDC power supply and contained five, normally-closed E-stop buttons wired in series. The loop controlled the power supplied to the solid-state relays (SSR's) which in turn controlled the power supplies located in the Relay cabinet. Upon pressing any of the five E-stop buttons, the SSR's opened and the power to the Relay cabinet was removed. This removed power to the fuel shutoff solenoid, located on the engine, and it closed. This also deactivated the fuel cart, as its control power was supplied by the Relay cabinet. A schematic of the E-stop loop is shown in Figure 5.

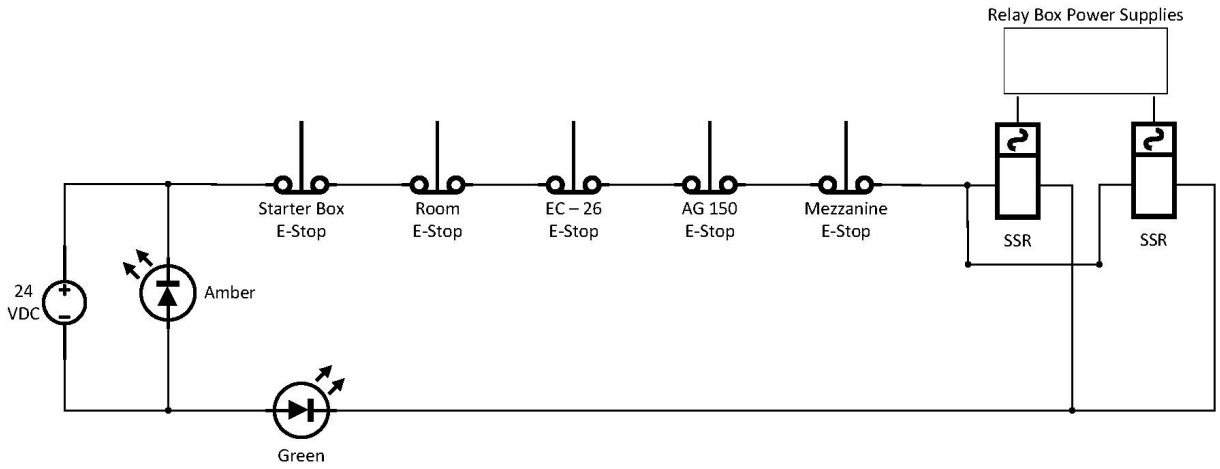

Figure 5: E-stop loop schematic

Basic Control System

The eddy current dynamometer was used to control the engine speed. A PID control loop within DynoMax was tuned for this particular engine application. PID settings were 20/10/15. The engine load (torque) was varied by changing the position of the load control lever on the engine. Control of the lever was managed through DynoMax using a stepper motor. PID settings were 3/1/1.

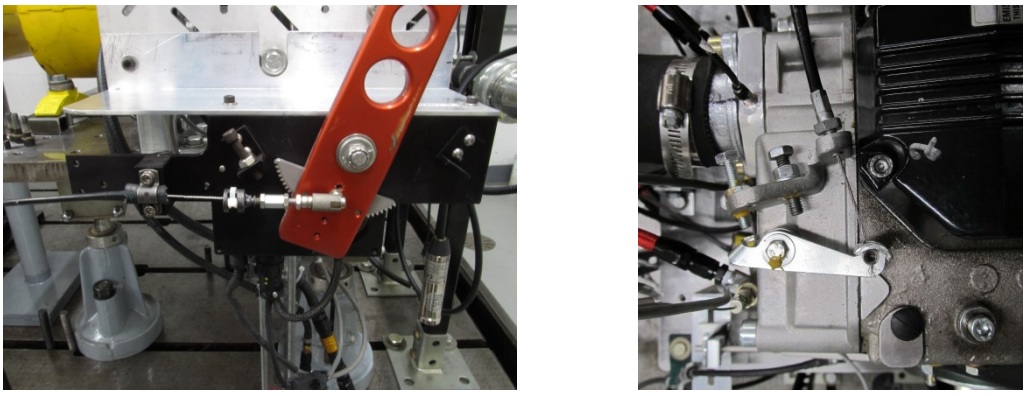

Figure 6: Load control lever (left) and engine connection point (right)

Engine Mounting

The engine was mounted directly to a 25.4 mm thick, A572 steel plate which was Blanchard ground on one side. Four setup clamps were used to attach the engine to the plate. A manufacturing drawing of the plate is shown in Figure 7.

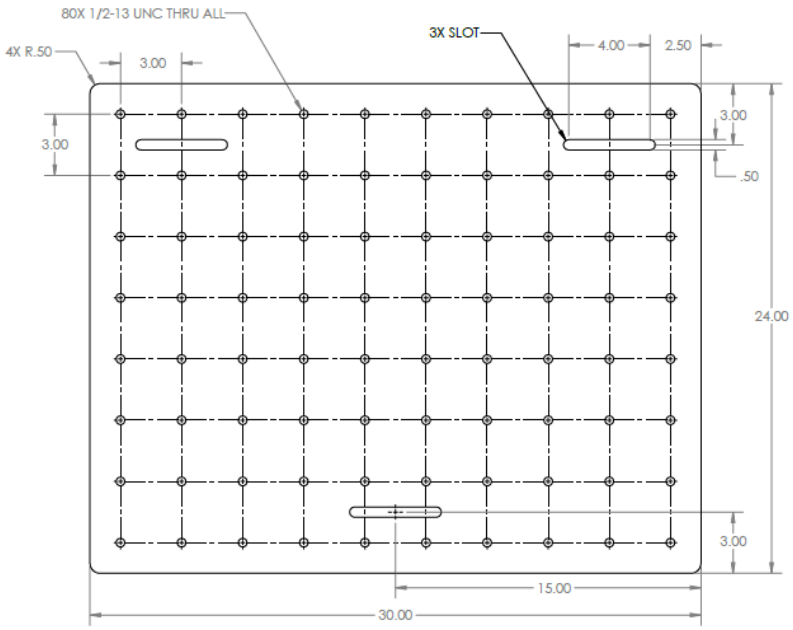

Figure 7: Engine mounting plate

The plate was supported by three elephant feet, each with a rubber isolator installed between the elephant foot and the plate. Figure 8 shows the installation for one of the isolators.

Figure 8: Engine isolation system

Engine and Dyno Cooling Systems

The engine was cooled using a 50/50 mix of propylene glycol and water, the stock integrated engine cooling pump, and a plate heat exchanger mounted near the engine on the bedplate. An engine cooling circuit diagram is shown in Figure 9.

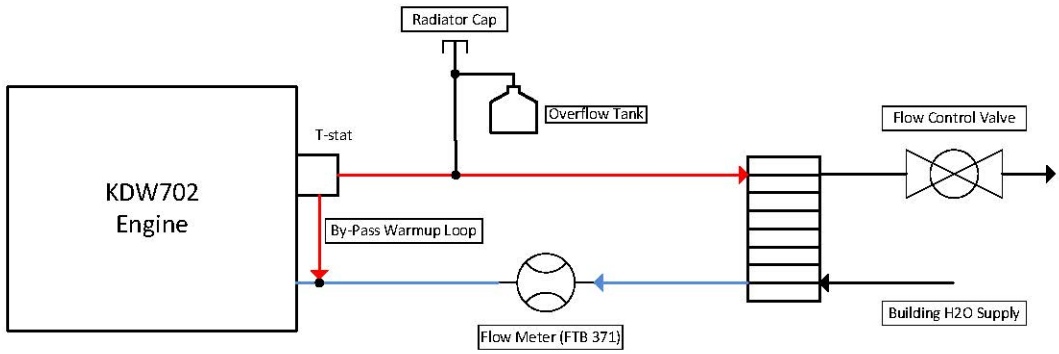

Figure 9: Engine cooling system schematic

A turbine-style flow meter was installed in the return line to measure coolant flow rate. The flow of building water through the heat exchanger was controlled using a normally-open flow control valve. The valve was PID controlled using DynoMax. Closed-loop control was utilized by monitoring the coolant-out temperature of the engine.

The eddy current dynamometer was cooled using a 30/70 mixture of propylene glycol and water and a plate-type heat exchanger. Building water flow rate through the heat exchanger was controlled using a flow control valve. The valve was PID controlled using DynoMax. Closed-loop control was utilized by monitoring the coolant-out temperature of the dyno. A schematic diagram of the dyno cooling system is shown in Figure 10.

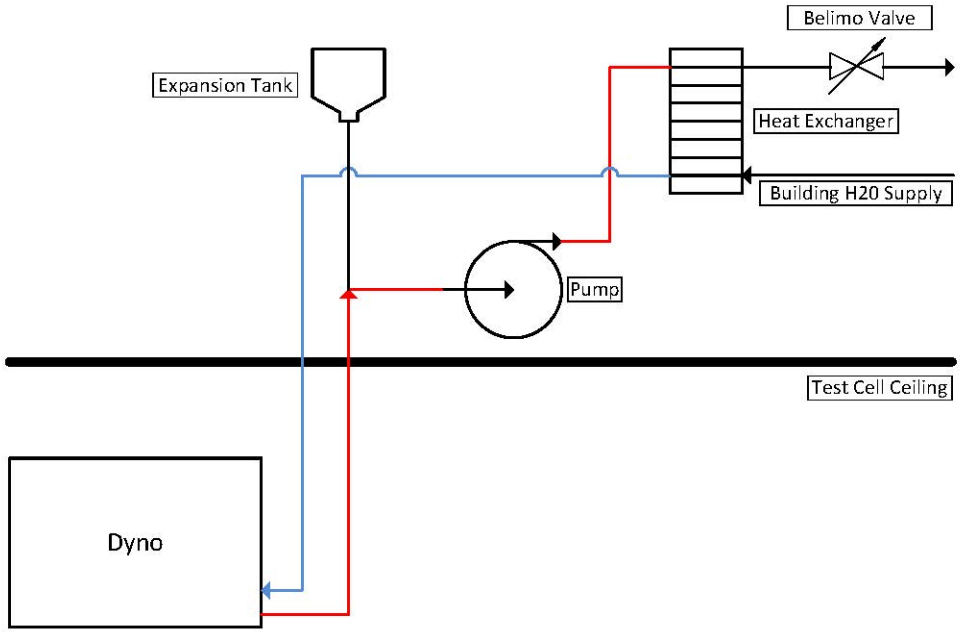

Figure 10: Dyno cooling system schematic

Engine Exhaust and Room Air Exchange System

A 4,000 CFM fan was utilized to extract exhaust gases from the test cell as well as exchange the air in the cell every 60 seconds. There was a dedicated, natural gas-fired make-up unit to

maintain room temperature at approximately 25°C. This was also the air the engine used for operation.

Fuel

The fuel utilized for the majority of the data collection was locally sourced off-road diesel purchased at a local Krist fuel station. The fuel was purchased in 10 gallon quantities at a time, from 12/2017 to 09/2018. A limited set of data (Phase 1.4) was acquired using F-24, which was supplied by A. Wiegand of TARDEC.

Intake Air Heater and Oil Pan Heater

An intake air heater (12 VDC @ 80 amps) was utilized to improve cold-start performance. Without the heater and glow plugs (replaced with cylinder pressure transducers), the engine was very difficult to start when cold (ambient temperature). The intake air heater was operated for ~30 seconds before engine starting to warm the intake air and provided adequate energy to the intake air to improve cold-start performance.

An oil pan heater was also added to reduce the time required to warm up the oil in the engine. This not only shortened the time to reach stable operating conditions, but also improved the cold-start performance of the engine.

Engine and Dynamometer Instrumentation

The engine and dynamometer were instrumented with various temperature, pressure, flow, and position sensors. Sensor details and locations are listed in Table 3. Note that cylinder pressure transducers were installed in the glow plug hole using a custom adaptor (Appendix 9).

Table 3: Engine instrumentation channel list

Channel	Sensor	Location
Ambient test cell temperature	Land-and-Sea thermistor	Above data acq. box
Ambient test cell pressure	Land-and-Sea transducer	Above data acq. Box
Ambient test cell RH	Land-and-Sea transducer	Above data acq. Box
Intake manifold temperature	Temprel 1/32” dia x 6” L ungrounded, k-type thermocouple, Inconel sheath, 72” lead wires	Intake manifold, before individual cylinder
Intake manifold pressure	Omega PX309 (Omega 0-30 psia)	Intake manifold, before individual cylinder
Cylinder pressure	PCB 115A04	Cylinder glow plug hole
Crankshaft location	AVL 365C, 0.1 CAD resolution	End of crankshaft, on accessory-drive side
Exhaust temperature	Temprel 1/32” dia x 6” L ungrounded, k-type thermocouple, Inconel sheath, 72” lead wires	Each cylinder exhaust port
Exhaust pressure	Omega PX309 (0-30 psia)	Each cylinder exhaust port
Exhaust oxygen concentration	EcoTron ALM with Bosch PLU4.9 sensor	In exhaust, located between cylinder and muffler

Coolant in temperature	Temprel 1/32” dia x 6” L ungrounded, k-type thermocouple, Inconel sheath, 72” lead wires	On engine, as coolant enters engine
Coolant out temperature	Temprel 1/32” dia x 6” L ungrounded, k-type thermocouple, Inconel sheath, 72” lead wires	On radiator cap fitting, approximately 1 meter from engine coolant outlet
Coolant block temperature	Temprel 1/32” dia x 6” L ungrounded, k-type thermocouple, Inconel sheath, 72” lead wires	In block, below exhaust manifold
Coolant flow	Omega FTB 371	Coolant return line to engine
Oil temperature	Temprel 1/32” dia x 6” L ungrounded, k-type thermocouple, Inconel sheath, 72” lead wires	In oil pan drain plug
Oil pressure	Omega PX309 (0-100 psig)	At valve cover
Fuel supply temperature	Temprel 1/32” dia x 6” L ungrounded, k-type thermocouple, Inconel sheath, 72” lead wires	Fuel supply to rail
Fuel supply pressure	Omega PX309 (0-30 psia)	Fuel supply to rail
Fuel return temperature	Temprel 1/32” dia x 6” L ungrounded, k-type thermocouple, Inconel sheath, 72” lead wires	At valve cover
Dyno speed	Froude-Hofmann Magnetic pickup	Shaft of dynamometer
Dyno torque	Sherborne Sensors T22-251 load cell	Dynamometer housing
Dyno cooling water flow switch	Froude-Hofmann	At dynamometer water outlet
Exhaust sample port (smoke)	AVL	Between exhaust port and muffler

Phase 0: Baseline Data

The engine was received new and thus it needed to be operated at a reduced speed and load condition for 50 hours, to properly break it in. Four different speeds over a range of loads were used to break the engine in, as shown in Table 4. These points were operated approximately equally until 50 hours was achieved.

Table 4: Engine break-in speed/load points

Engine Speed	Engine Load (Nm)
1800 RPM	5
2400 RPM	5, 15, 25
2800 RPM	5, 15, 25
3200 RPM	5, 25

At no time did the load exceed 75% of rated torque, per the user manual break-in limit.

Because the engine was equipped with cylinder pressure transducers, real-time observation of individual cylinder work output (gross indicated mean effective pressure (GIMEP)) and combustion stability (coefficient of variation (COV) of GIMEP) was possible. It was observed that cylinder 2 was producing less work output and had a higher COV of GIMEP compared to cylinder 1 during initial shake down and before baseline data was collected. The engine manufacturer was contacted about the situation and a new injector was supplied under warranty. The injector was installed and the work output was adjusted by changing the fuel injector rack setting for cylinder 2. The procedure was provided in the KDW702 service manual, which is available here: http://resources.kohler.com/power/kohler/enginesUS/pdf/KDW702_1003_1404_SM_EN.pdf .

The following test matrix (Table 5) was used to collect the Phase 0 baseline data.

Table 5: Engine speed and load test matrix for Phase 0

Engine Speed	Engine Load (Nm)
1800 RPM	2.7, 9.7, 18.7, 29.2, 38.3
2400 RPM	2.8, 9.8, 20.3, 30.4, 41.8
2800 RPM	3.0, 10.0, 20.6, 30.3, 39.4
3000 RPM	3.4, 10.7, 20.5, 31.7, 37.2
3600 RPM	3.8, 9.2, 16.4, 24.4, 33.7

Summary of baseline results

Baseline test results were consistent with data provided by Kohler and Lombardini for this engine. Power, smoke, and exhaust gas temperature were in-line with the data provided by the manufacturer. The following six figures show the baseline testing results.

Dynamometer

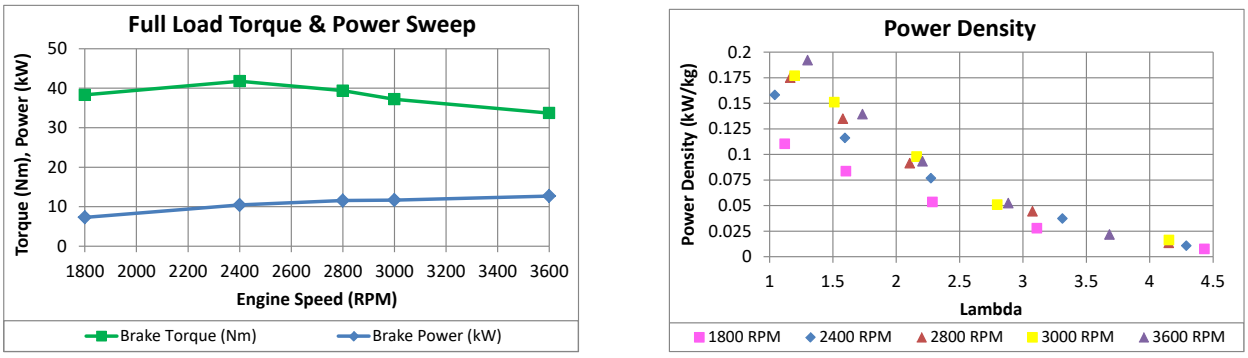

Figure 11: Phase 0 full load power & torque and power density

Filter Smoke Number

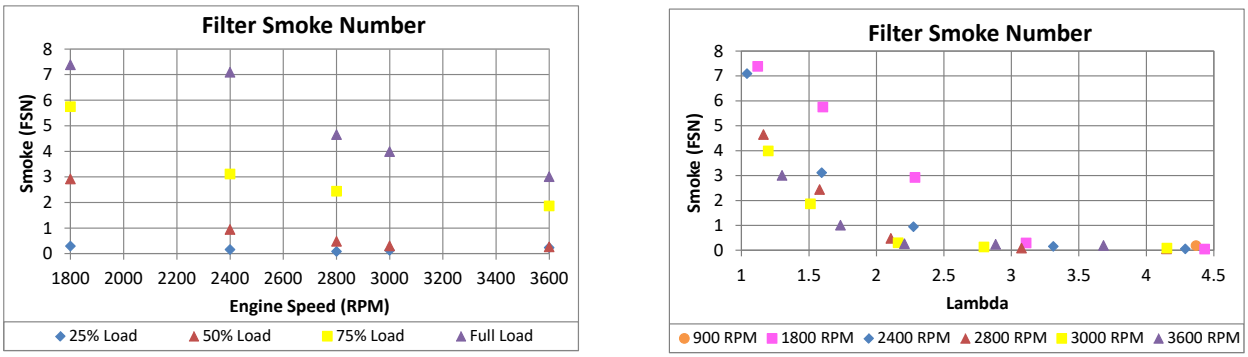

Figure 12: Phase 0 filter smoke number

Energy Distribution

Note: fuel power was calculated based on the measured fuel flow rate (kg/hr) and lower heating value of the fuel.

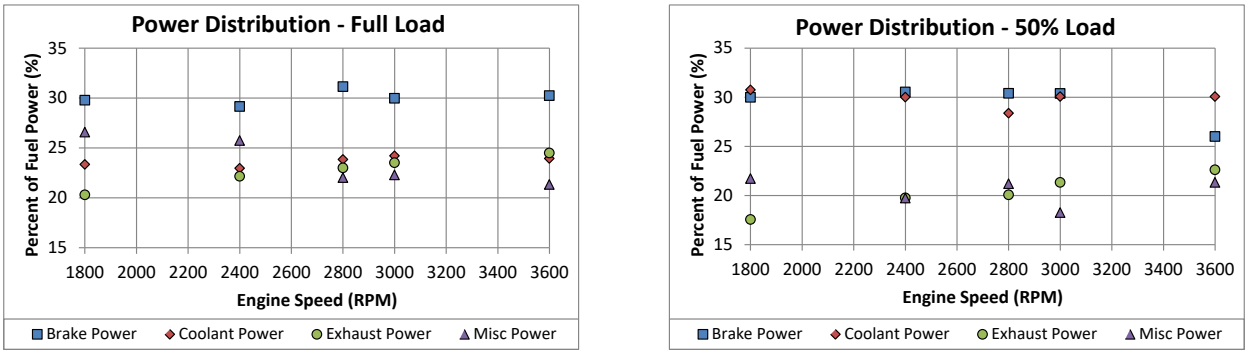

Figure 13: Phase 0 fuel power distribution at full load (left) and 50% load (right)

Combustion

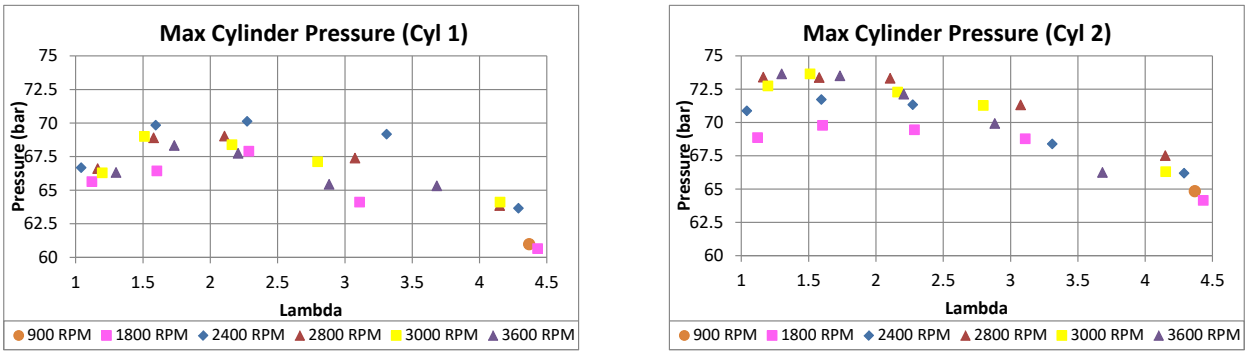

Figure 14: Phase 0 maximum cylinder pressure for cyl 1 (left) and cyl 2 (right)

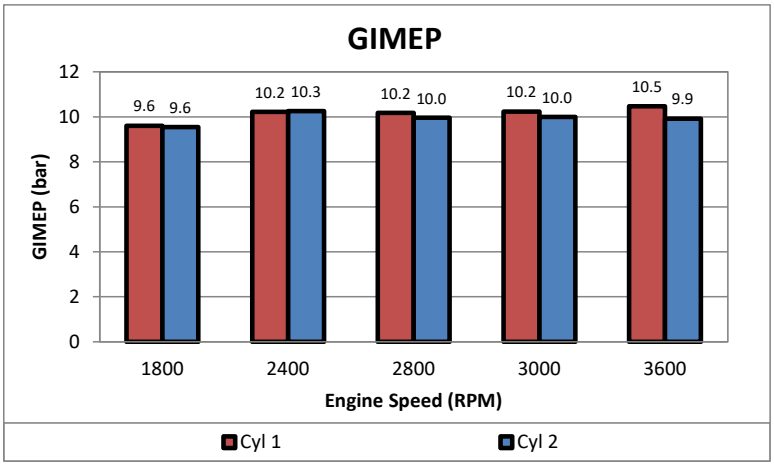

Figure 15: Phase 0 gross IMEP cyl-to-cyl comparison at full load

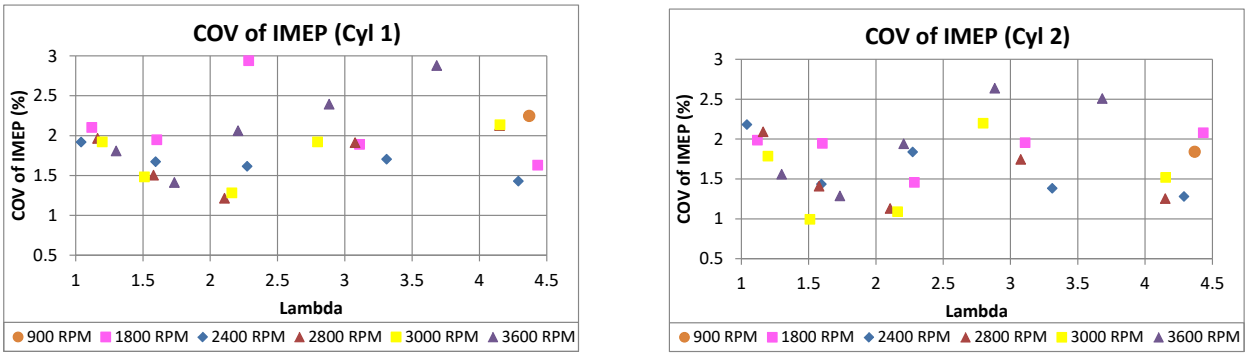

Figure 16: Phase 0 combustion stability for cyl 1 (left) and cyl 2 (right)

Phase 1: Naturally-aspirated Operation

The test results for Phases 1.1, 1.2, and 1.4 are discussed in the Comparison Section of this report. The evaluation rational, procedures, limits, and the volumetric efficiency test (a standalone effort) results (Phase 1.3) are discussed in this section.

Prior to applying boost to the intake manifold, changes to the fuel delivery were made to study the impact on performance, combustion, and smoke output. Additional fuel was first added, but an increase in exhaust gas temperature required a change in injection timing (injection advance). A brief study on the impact of the intake components was performed and a very limited set of data was acquired while operating on F-24.

Operational Limits

Per the recommendation from Kohler and Lombardini, the maximum exhaust temperature was not to exceed 650°C and the maximum cylinder pressure was not to exceed 110 bar.

Phase 1.1: Fuel Delivery Adjustment

Initially, attempts were made to adjust fueling using the limit screw on the injector rack. This was moderately consistent, but there was the risk of losing the set point reference. After some discussion it was decided that since the goal was to compare the effects of changes in quantity of fuel, this ultimately correlates with air-to-fuel mass ratio, “lambda”. Thus a procedural change was made to compare data using lambda as the independent variable. The fuel screw was turned in (up) 3 full turns from the factory setting so it no longer influenced the fueling operation of the engine. The fuel screw is shown circled in red, in Figure 17. This also effectively eliminated the speed governor on the engine as this limit screw is a part of the centrifugal governor system.

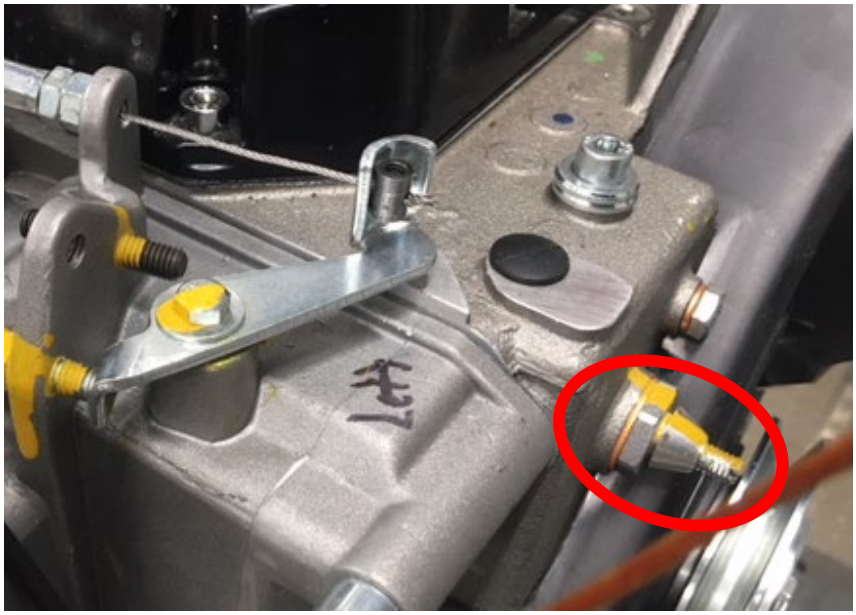

Figure 17: Fuel limit screw

Phase 1.2: Fuel Injection Timing

Fuel injection timing was advanced to reduce exhaust gas temperature as fueling quantity increased. The setting procedure used is shown in Figure 18, where a dial indicator and reference fixture were utilized to measure the injector timing screw for each adjustment. The measurement was made when the injector arm was riding on the non-injecting portion of the camshaft (low point on the cam lobe).

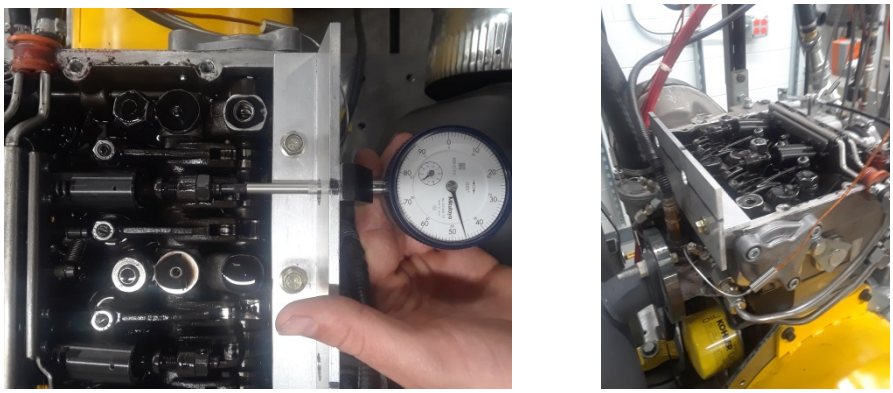

Figure 18: Fuel injector timing adjustment and fixture

The following injection advance settings were evaluated.

- 0.25 turns in
- 0.50 turns in
- 0.625 turns in
- 0.75 turns in
- 1.0 turns in

Advancing the injection timing had a direct impact on reducing exhaust gas temperature. However, advance settings of 0.75 and 1.0 resulted in unstable operation of cylinder 2, when the engine was operated above 3000 RPM. Upon trial and error, it was determined that an injection advance of 0.625 turns in from the stock setting resulted in a measureable decrease in exhaust gas temperature yet did not affect the cylinder 2 operation. Therefore, a final setting of 0.625 turns in from the stock position was utilized to reduce the exhaust gas temperatures at the higher fueling quantities, under naturally-aspirated operation.

Phase 1.3: Volumetric Efficiency Study

Three intake configurations, as shown in Figure 19, were studied to determine if the intake air heater and/or intake air filter caused significant restriction in the flow of air into the engine. It was important to minimize the variability in the intake manifold temperature during this testing, as it directly affects the intake manifold density. The intake manifold temperature ranged from 29°C to 31°C for the volumetric efficiency tests.

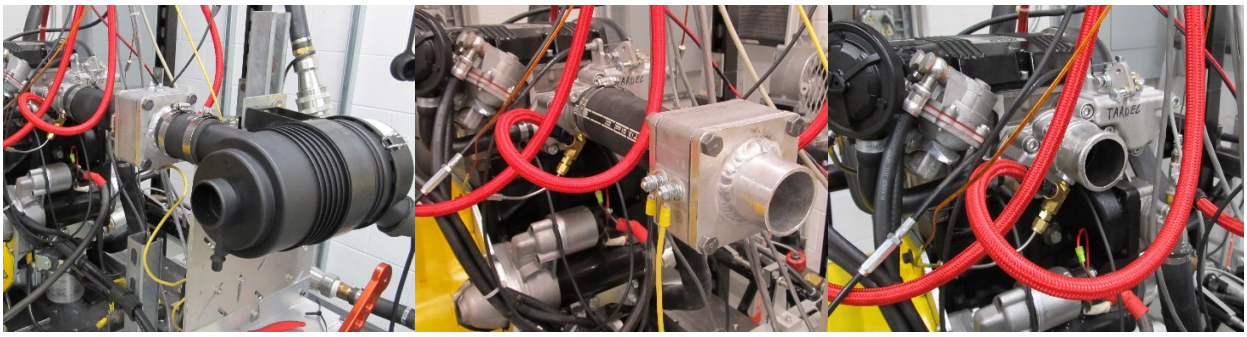

Figure 19: Intake system configurations: full (left), heater (center), open (right)

Volumetric efficiency was computed using the following equation:

$$\eta_v = \frac{2 * \dot{m}_{fuel} * AFR}{\left(\frac{P_{man}}{RT_{man}}\right) * V_D * RPM}$$

As shown in Figure 20, no significant difference (less than 5%) in volumetric efficiency was observed between the full system and the components removed. In fact, the intake system consisting of the intake heater and air filter typically produced the highest volumetric efficiency.

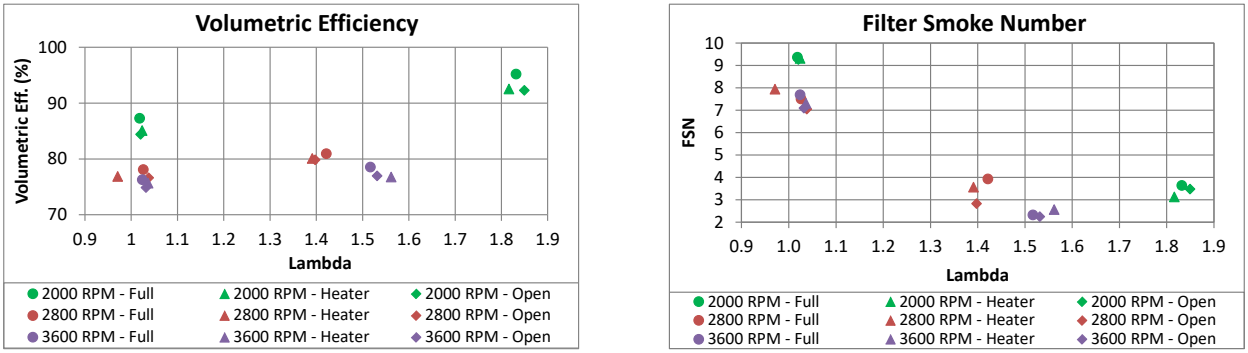

Figure 20: Phase 1.3 volumetric efficiency results

Because the air flow does not appear to be affected by the intake air heater or the air filter, changes to engine performance parameters, such as filter smoke number, were expected to be minor. As shown in Figure 20, no clear trend between FSN and intake configuration was observed.

Phase 1.4: Evaluation of F24

A fuel change to F24 was performed, to study the impact on performance, combustion, and efficiency. The provided F-24 likely had a lower cetane compared to the off-road diesel fuel (DF2) which was utilized for the majority of this project, though this was not validated with fuel analysis.

Four speed/load points were used to evaluate the impact of F-24 on maximum torque and power, BSFC, smoke, combustion timing, and stability. The test matrix used to evaluate F-24 is shown in Table 6.

Table 6: Test matrix to evaluate impact of F-24

Engine Speed (RPM)	Engine Load (Nm)	Lambda
2800	10.5	n/a
2800	40	1.0
3600	25	n/a
3600	39	1.0

Phase 2: Boost Analysis

Intake air boosting was explored for two engine speeds, which approximately represented peak torque and peak power for this engine. At each engine speed, either a lambda value or a load value was used as the target, as shown in Table 7.

Table 7: Phase 2 boost evaluation test matrix*

Engine Speed	Target Lambda	Actual Lambda	Target Load (Torque)	Actual Torque	Actual Boost Pressure	Theoretical Boost Power from a Mechanical Supercharger
[RPM]	-	-	[Nm]	[Nm]	[psig]	[W]
2000	1.0	1.02	n/a	40.8	1.11	112
2000	n/a	1.19	38	37.6	1.14	118
2000	1.0	1.03	n/a	44.9	2.24	237
2000	n/a	1.35	38	39	2.33	263
2000	1.0	1.04	n/a	49.4	2.75	304
2000	n/a	1.48	38	37.9	2.91	315
2000	1.0	1.03	n/a	56.2	4.74	595
2000	n/a	1.70	38	37.9	4.69	567
3600	1.0	1.05	n/a	44.2	1.41	237
3600	n/a	1.29	38.5	38.7	1.43	244
3600	1.0	1.06	n/a	47	2.2	390
3600	n/a	1.37	38.5	38.9	2.12	380
3600	1.0	1.09	n/a	48.9	2.92	594
3600	n/a	1.44	38.5	38.0	2.98	584
3600	1.0	1.09	n/a	52.6	4.09	785
3600	n/a	1.55	38.5	38.8	4.58	875
3600	1.0	1.14	n/a	56.6	5.93	1484
3600	1.0	1.20	n/a	62.7	8.42	2323

*Note: Values shown as “n/a” were uncontrolled. Either a lambda target or a load target was used, not both.

The injection timing was set to the original, stock value (no advance). Boosting was accomplished by supplying compressed air from a high output building air compressor directly to the intake manifold of the engine.

The power required to increase the intake air pressure was estimated using conservation of energy for a control volume. It was assumed that a supercharger was to provide the boost to the engine in actual operation and that the only impact from the boost mechanism was the increase in flow potential (Pv). In addition, the system was assumed well-insulated, so heat transfer with the environment was negligible. The efficiency of the supercharger was assumed to be 65%. Table 7 shows the estimates for the power required to provide the boosted air. It is important to note that if a turbocharger was utilized to boost the intake air pressure, instead of a supercharger, the power loss would be reduced but not completely eliminated due to the increased back-pressure of the turbine in the exhaust stream.

A hi-speed, piezo-resistive pressure transducer was installed in the intake track of the engine, to observe the pressure fluctuations during boosting. A plot of one of the tests is shown in Figure 21. From the plot it is observed that the mean intake pressure increased with increased boost, as expected. However, the fluctuating component of the pressure, at a set engine speed did not change significantly, as intake pressure was increased. The frequency content at 3600 RPM was measurably higher compared to 2000 RPM.

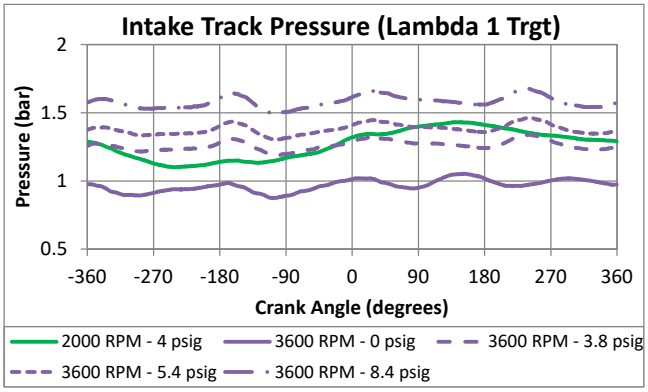

Figure 21: Phase 2 intake track pressure fluctuations

Phase Comparisons

This section compares the various phases of engine testing, from the baseline (Phase 0) up to and including additional intake air pressure (Phase 2). Table 8 shows the different progressions of engine settings as the fueling, injecting timing, fuel composition, or boost were changed.

Table 8: Phase comparison

	Phase 0	Phase 1.1	Phase 1.2	Phase 1.4	Phase 2
Fuel	DF2	DF2	DF2	F-24	DF2
Fuel Quantity	Stock	Additional	Additional	Additional	Additional
Fuel Timing	Stock	Stock	Advanced	Advanced	Stock
Boost	N/A	N/A	N/A	N/A	Yes

Power

Figure 22 shows the brake power produced by the engine with lambda equal to approximately 1.0. From the figure, the following conclusions can be drawn:

- Additional fueling (Phase 1.1) resulted in more power output as the engine speed increased.
- The advance in injection timing (Phase 1.2) resulted in a loss in power at lower speeds but an increase in power at the higher speeds. This impact is due to a shift in the combustion phasing.
- F-24 (Phase 1.4) resulted in no noticeable power change from Phase 1.2. This was an expected result due to the constant lambda target.
- For Phase 2, the following conclusions can be drawn:
    - The engine was not able to achieve 1.0 lambda due to either the exhaust gas temperature limit or because the maximum injector flow rate (rack position) was reached. The rack limit was reached at ~9 psig of boost.
    - Theoretically, additional fuel could be added to produce more power, if the injectors could flow more fuel.
    - The maximum brake power was 21.2 kW @ 3600 RPM with 8.4 psig of intake air pressure. This value takes into account the loss from a supercharger to generate the boost (2.3 kW). The net power increased 67% compared to the stock engine.

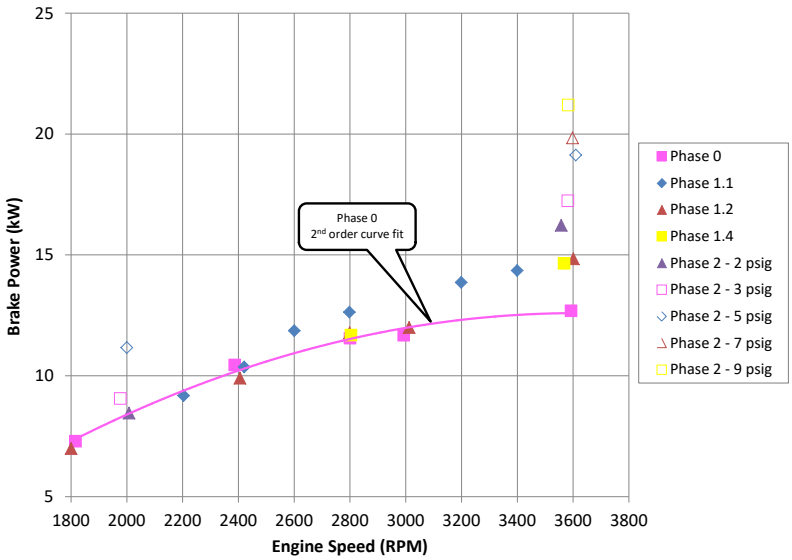

Figure 22: Brake power vs engine speed for Phase 0, 1.1, 1.2, and 2 (all at Lambda ~= 1.0)

Figure 23 shows the brake power plotted against lambda. As expected, power increases as fuel increases (lambda decreases). The trends identified in Figure 22 are clearly observed in this figure as well.

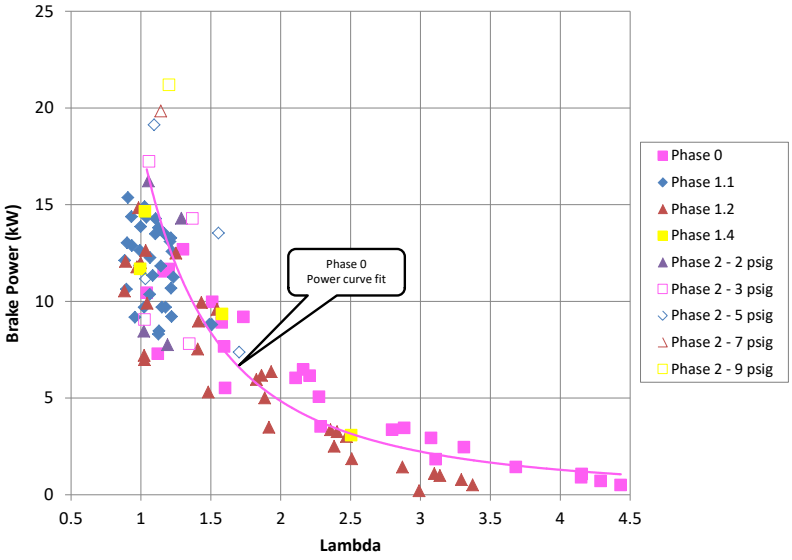

Figure 23: Brake power vs lambda for Phase 0, 1.1, 1.2, 1.4, and 2

Power Density

The primary goal of this project was to increase the power density of a small, compression-ignition engine. Figure 24 shows the power density for the various phases. Phase 2 data takes into account the power required by a supercharger to provide the increased air pressure. From the figure, the following conclusions can be drawn:

- Increasing the fuel injection (Phase 1.1) improved the power density slightly, but only with lambda values less than 1.
- Advancing the injection timing (Phase 1.2) at the higher lambda values (lighter load) reduced the power density, due to less-optimal combustion phasing. Little to no effect on the power density was observed near lambda 1.0.
- F24 (Phase 1.4) produced similar power density values compared to Phase 0.
- Boosted (Phase 2) operation produced the highest power density of 0.32. Compared to the stock peak power density of 0.19, this was a 68 % increase.

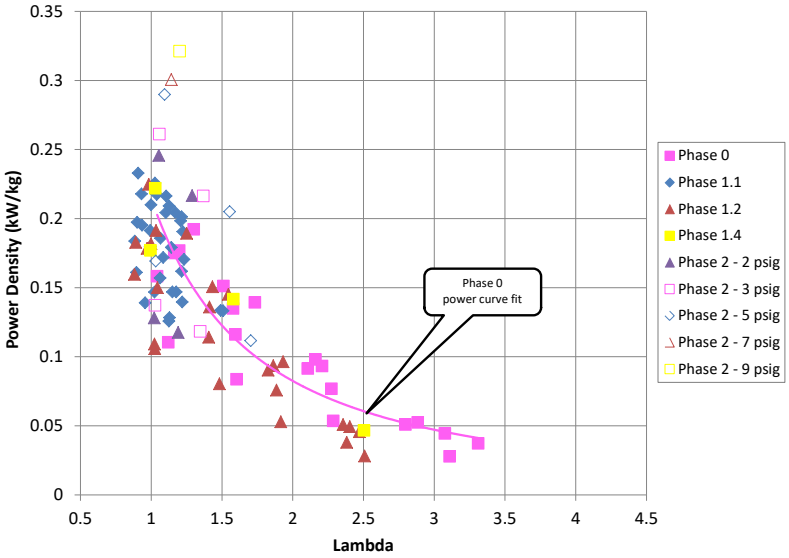

Figure 24: Power density vs lambda for Phase 0, 1.1, 1.2, 1.4, and 2

BSFC

Figure 25 shows the brake specific fuel consumption versus lambda, for the various phases evaluated. For Phase 2, the supercharger power was accounted for in this data. The plot reveals the following information about BSFC:

- Increasing the fuel injection quantity (Phase 1.1) had a minimal effect on BSFC although the range of lambda values was not as large as compared to Phase 0.
- Advancing the injection timing (Phase 1.2) tended to increase BSFC compared to Phase 0, especially at the higher lambda values (lighter engine loads). This is the result of poor combustion phasing and thus a loss in work output from the fuel.
- F-24 (Phase 1.4) did not appear to significantly impact BSFC compared to Phase 1.2.
- The common BSFC “hook” is clearly identified in the Phase 0 and Phase 1.2 data sets, with a minimum BSFC occurring around a lambda of 1.5 for all test conditions. The lowest BSFC (249 g/kW-hr) occurred at lambda = 1.5 for Phase 0.

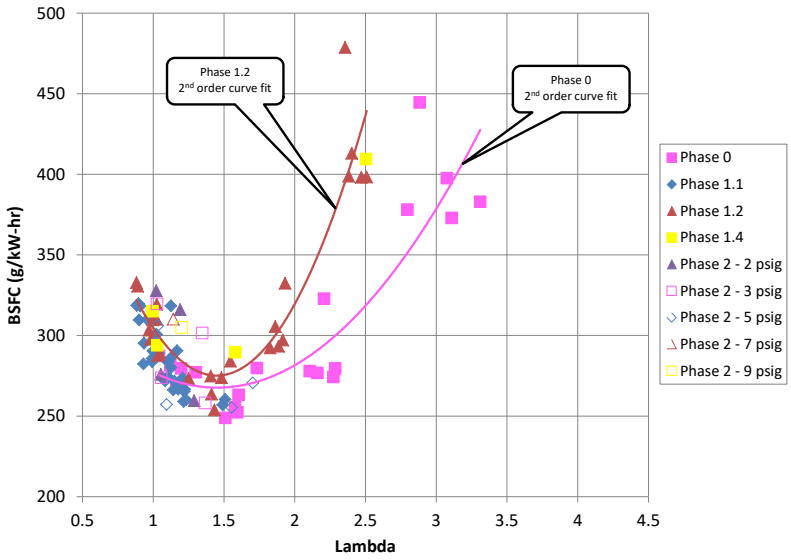

Figure 25: BSFC comparison for Phase 0, 1.1, 1.2, 1.4, and 2

Smoke

Figure 26 shows the smoke produced from the engine, as a function of lambda. From the figure, the following conclusions are drawn:

- The lowest smoke values (~0.05) occurred with the stock configuration and highest (most fuel lean) lambda values (>4).
- A clear relationship between smoke and lambda is observed. As lambda increases, regardless of injection timing or intake air pressure, smoke production reduced. As injection quantity increased (Phase 1.1), smoke significantly increased.
- Smoke increased as injection timing was advanced (Phase 1.2), but not as significantly as with injection quantity.
- F-24 (Phase 1.4) did not produce significantly more or less smoke compared to other fuel delivery modifications.
- Boosting (Phase 2) tended to reduce smoke production, but not to the levels observed in the stock configuration.

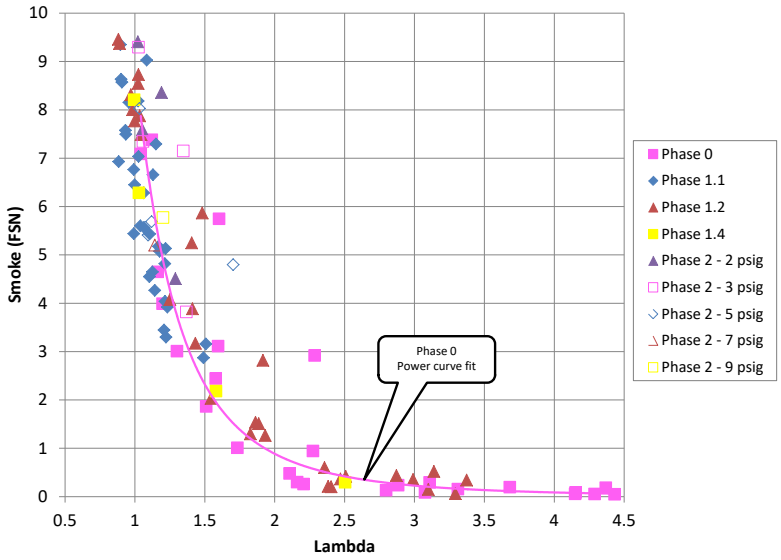

Figure 26: Smoke output vs lambda for Phase 0, 1.1, 1.2, 1.4, and 2

Exhaust Gas Temperature

Figure 27 shows the exhaust gas temperature as a function of lambda. From the figure the following conclusions are drawn:

- A clear relationship between exhaust gas temperature and lambda exists. As lambda increases, EGT decreases.
- On average, EGT reduced with additional fueling (Phase 1.1) compared to the stock configuration at a nearly constant lambda value of 1.1.
- EGT decreased with an advance in injection timing (Phase 1.2), as expected. This permitted operation at a smaller lambda (richer) and thus more power at higher engine speeds, without exceeding the EGT limit.
- EGT was not affected by the switch to F-24 (Phase 1.4), when compared to Phase 1.2
- Lambda 1.0 operation was not possible at 3600 RPM and 5 psig, 7 psig, and 9 psig of boost (Phase 2) because the EGT limit (650°C) would have been exceeded.
    - Changes to injection timing to reduce EGT were not explored due to time constraints

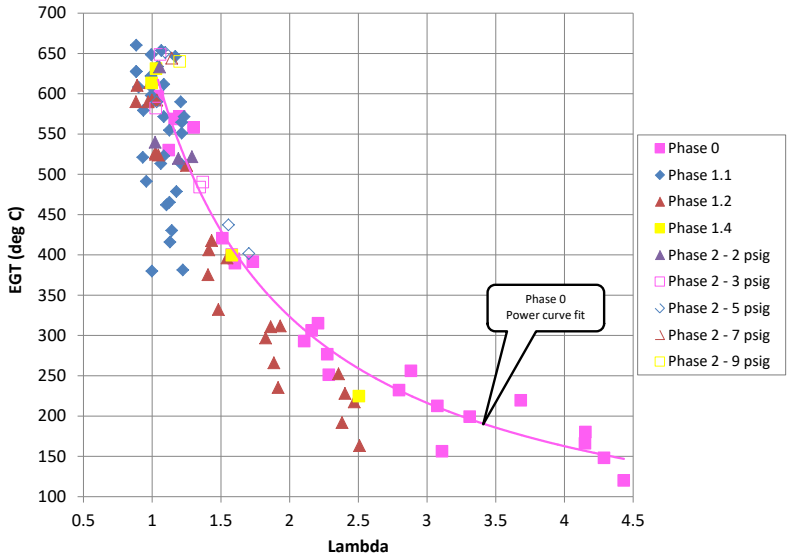

Figure 27: EGT (cyl 1) vs lambda

Energy Balance (fraction of fuel energy)

An energy balance analysis was performed, to track the flow of fuel energy to four primary paths which were crankshaft, coolant, exhaust, and miscellaneous. Miscellaneous was computed as the different between the fuel energy and the sum of the crankshaft, coolant, and exhaust energy. The results are included in the appendices and the following conclusions are drawn:

- Coolant heat rejection was similar for all test cases.
- For F24 (Phase 1.4), the exhaust energy was higher for F24.
- As boost increases (Phase 2) at 3600 RPM:
    - Consistent increase in brake power over the range of boost levels tested
    - Limited change in coolant energy
        - Enleanment with boost may have affected this
    - A higher percentage of fuel energy was transferred to the exhaust as boost pressure increased
        - It would be expected that a higher percentage of the fuel energy would be in the exhaust if lambda was able to be maintained at 1.0 at the higher speeds and boost levels.
    - Miscellaneous energy increased with boost pressure, which represents radiant heat loss, convective heat loss, and friction.

Maximum Cylinder Pressure

Figure 28 shows the peak pressure versus lambda for the various phases tested. From the figure, the following conclusions are drawn:

- Peak cylinder pressure was fairly constant over a wide range of lambda values for the baseline condition (Phase 0). This may be a result of the indirect injection system and the location of the in-cylinder pressure measurement.

- Additional fueling (Phase 1.1) did not impact peak cylinder pressure although the range of lambda values was limited compared to Phase 0.
- Peak cylinder pressure increased with injection advance (Phase 1.2) with maximum increases exceeding 30%.
- Peak cylinder pressure reduced with F24 (Phase 1.4) compared to DF2 and advanced injector timing (Phase 1.2). This was more than likely due to a longer ignition delay and thus later combustion as a result of lower cetane number. The impact was fairly low and may be affected by the injection technology (IDI).
- The average peak cylinder pressure was maintained below the 110 bar pressure limit for all boost conditions tested. The highest average pressure measured was 106 bar at 8.4 psig of boost.

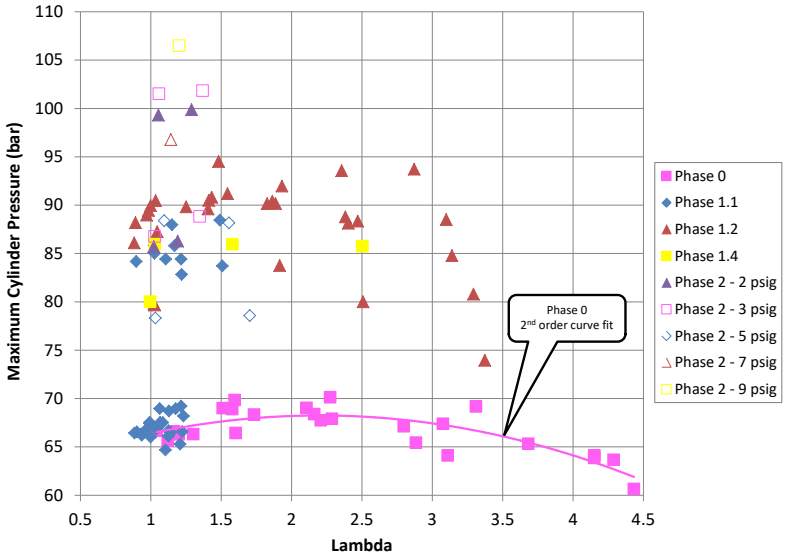

Figure 28: Maximum cylinder pressure (cyl 1) vs lambda

Combustion Duration (D10-90)

Figure 29 shows the combustion duration for the various phases tested. From the figure, the following conclusions are drawn:

- Decreasing lambda increases combustion duration due to additional fuel and thus power output.
- Additional fueling (Phase 1.1) resulted in longer combustion duration.
- Advancement of injection timing (Phase 1.2) produced some of the longest combustion durations at the lowest lambda values.
- F-24 (Phase 1.4) followed the combustion duration trend with lambda.
- No clear trend between combustion duration and intake air pressure (Phase 2) was observed.

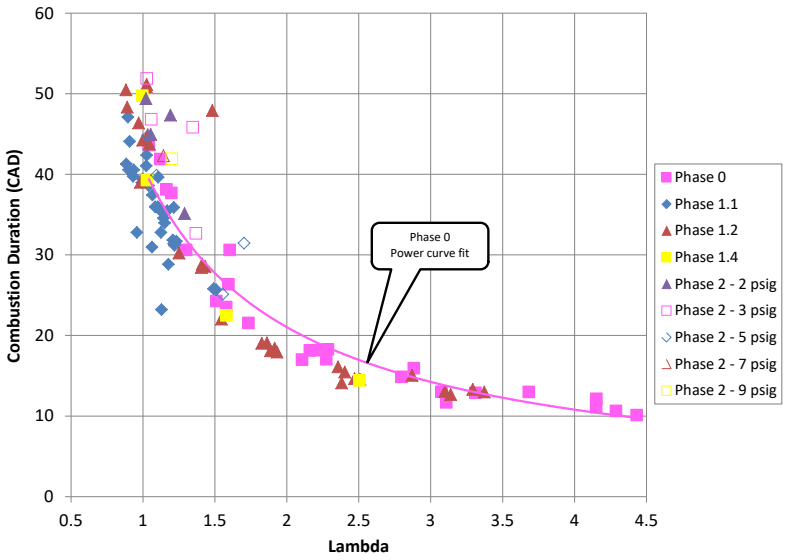

Figure 29: Combustion duration (D10-90, cyl 1) comparison

Combustion Phasing

Figure 30 shows the effect of the different phases on the CA50 location. From the figure the following conclusions are drawn:

- As lambda decreases, a general trend of later CA50 is noted.
- Additional fueling (Phase 1.1) results in similar CA50's at the lowest Phase 0 lambda values.
- Advanced injection timing (Phase 1.2) clearly advanced the CA50 timing, as expected.
- Combustion phasing shifts later with F-24 (Phase 1.4) compared to Phase 1.2.
- No clear trend in CA50 with boosting (Phase 2) was noted.

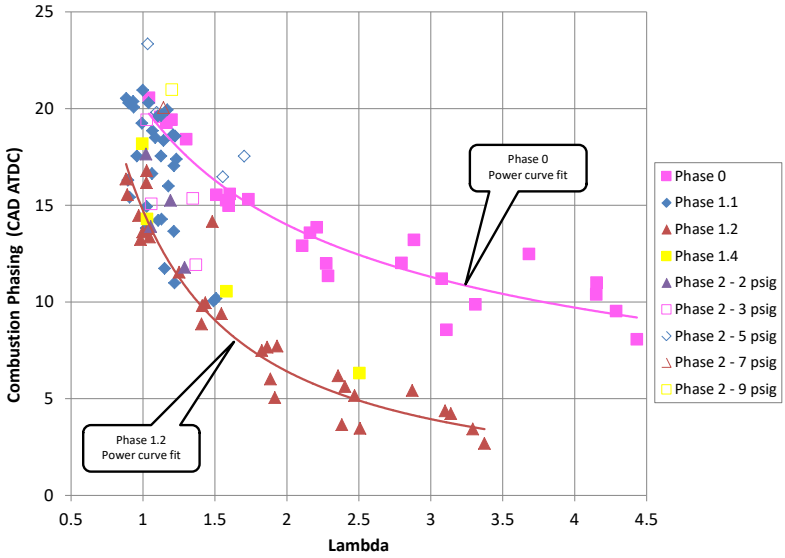

Figure 30: Combustion phasing (CA50 – cyl 1) vs lambda

Combustion Stability

Figure 31 shows how combustion stability changed as the various phases were tested. From the figure, the following conclusions are made:

- As lambda increased, a slight increase in the combustion instability occurred for Phase 0.
- No clear trend was observed in COV with modifications to injection quantity (Phase 1.1), timing (Phase 1.2), or boost (Phase 2).
- Combustion stability slightly degraded with F-24 (Phase 1.4) at lower lambda values, but the average value was less than ~2%.

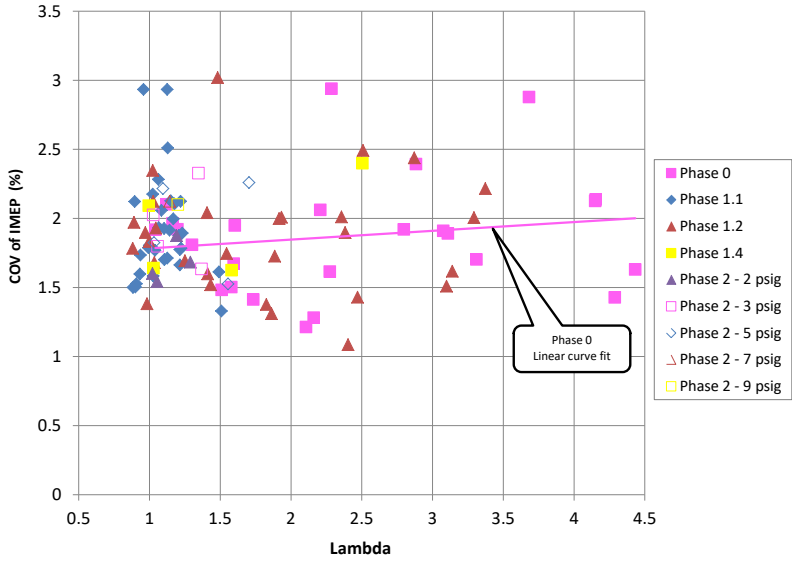

Figure 31: COV of IMEP (cyl 1) vs lambda

Conclusions

An increase in power density of a commercial, off-the-shelf, compression ignition engine was demonstrated using different techniques. The most effective was additional intake air pressure (boost), where up to 8.4 psig of boost was applied and the power density was increased 68%. Further increases in power density were not possible due to an injector flow rate limitation. Additional intake manifold air pressure along with more fuel would result in even higher power density but would require modifying the injection timing to keep EGT's below the operational limit.

Indirect injection provides an engine that is not only fuel-tolerant but also air/fuel ratio tolerant. Minimal impact on performance parameters was observed when switching from DF2 to F24 fuel. A fairly wide range of air/fuel ratios were tested with minimal impact on combustion stability or duration. Although indirect injection engines are less thermodynamically efficiency, the fuel delivery technology provides distinct advantages in terms of on-demand load capacity. This makes this engine design a strong candidate for highly intermittent power surges in application operation. It is conceivable that the engine could be utilized for light-duty operation and then when demand requires more power, calibration could be switched and the same engine could provide the necessary power, without significant modification to the overall engine structure or hardware.

Appendix 1: Work Directive Objective

The contractor shall demonstrate a power density increase on a commercial engine while operating on heavy fuels (JP8 and diesel). Existing literature shall be used to down-select appropriate technologies to achieve the engine operational objectives. The contractor shall evaluate a baseline engine to establish performance and efficiency metrics. The contractor will modify the baseline engine to achieve acceptable operation on heavy fuels with high power density and then document the impacts of various technologies. An analysis of the existing engine dynamometer test cell at MTU will also be performed, to highlight hardware and software selection, as well as provide recommendation for modifications for future installations.

Appendix 2: Nomenclature

- ATDC: After Top Dead Center
- BSFC: Brake Specific Fuel Consumption
- CAD: Crank Angle Degree
- CFM: Cubic Feet per Minute
- COV: Coefficient of Variation
- DAQ: Data Acquisition
- EGT: Exhaust Gas Temperature
- FSN: Filter Smoke Number
- GIMEP: Gross Indicated Mean Effective Pressure
- MFB: Mass Fraction Burned
- MSI: Machine Service Inc.
- PID: Proportional, Integral, Derivative Controller
- ROHR: Rate of Heat Release
- SOC: Start of Combustion

Appendix 3: Phase 0 – Baseline Data

Dyno Data

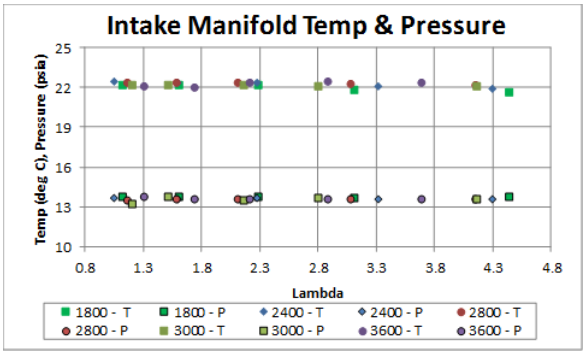

Figure 32: Phase 0 T_{intk_mnfld} & P_{intk_mnfld}

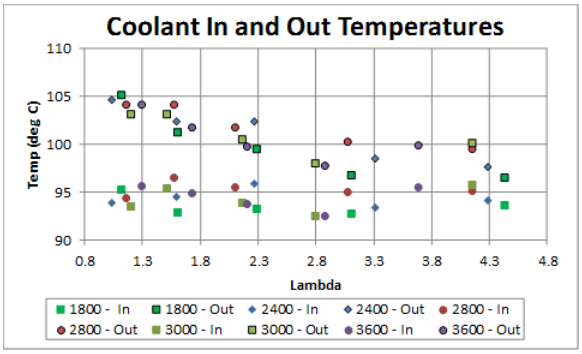

Figure 33: Phase 0 coolant temperatures

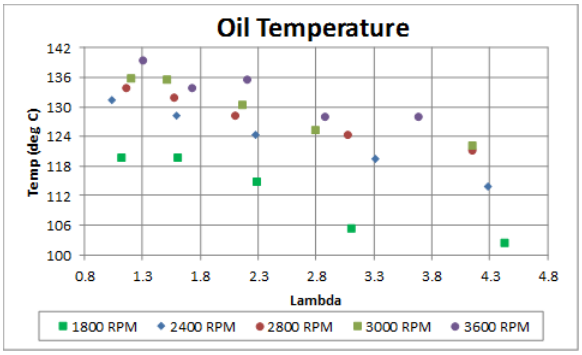

Figure 34: Phase 0 oil temperature

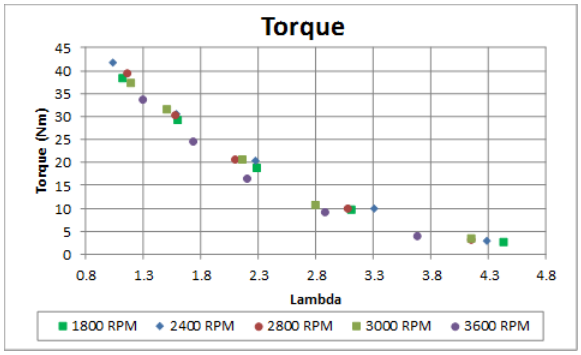

Figure 35: Phase 0 brake torque

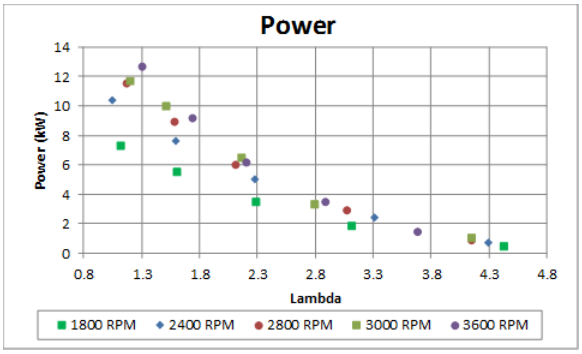

Figure 36: Phase 0 brake power

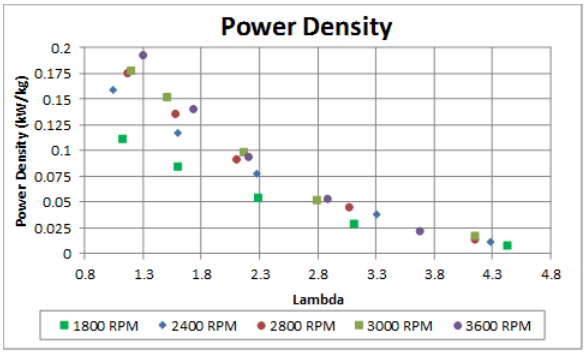

Figure 37: Phase 0 power density

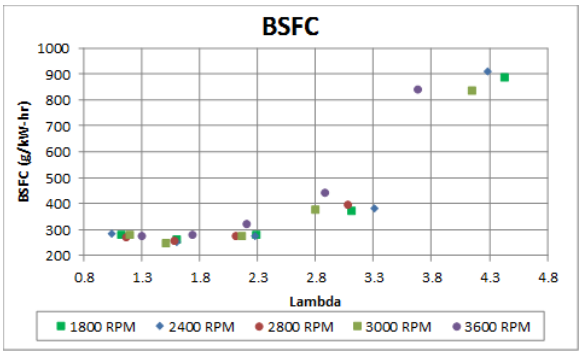

Figure 38: Phase 0 BSFC

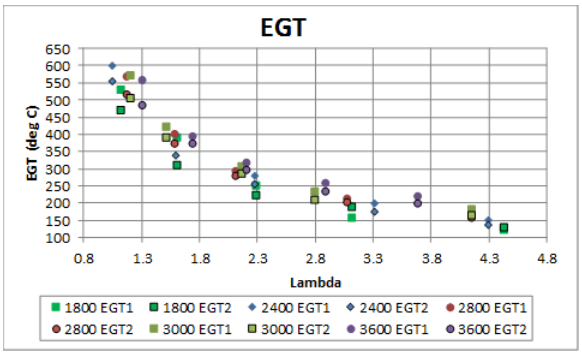

Figure 39: Phase 0 exhaust gas temperature

Fuel Energy Distribution Data

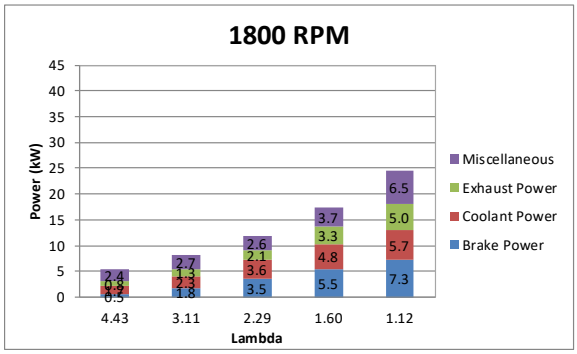

Figure 40: Phase 0 energy distribution @ 1800 RPM

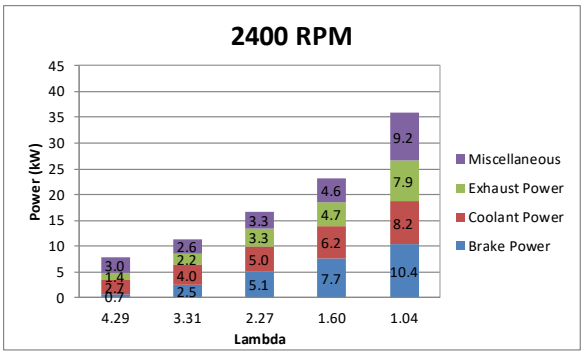

Figure 41: Phase 0 energy distribution @ 2400 RPM

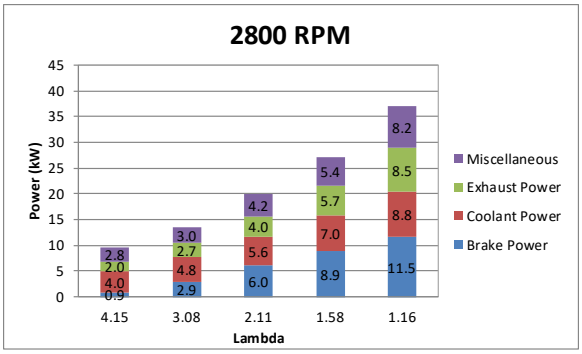

Figure 42: Phase 0 energy distribution @ 2800 RPM

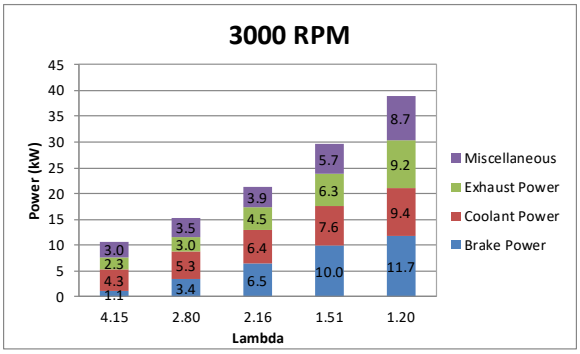

Figure 43: Phase 0 energy distribution @ 3000 RPM

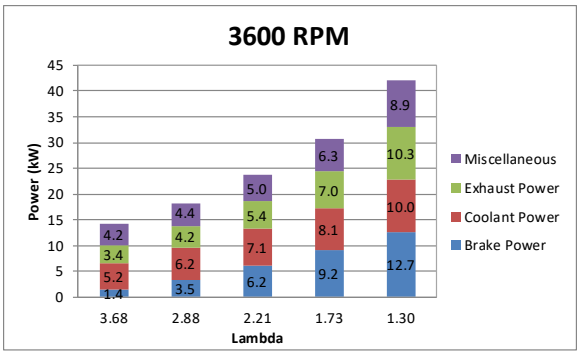

Figure 44: Phase 0 energy distribution @ 3600 RPM

Smoke Data

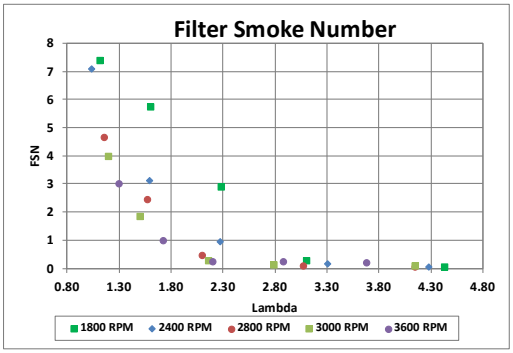

Figure 45: Phase 0 filter smoke number

Combustion Data

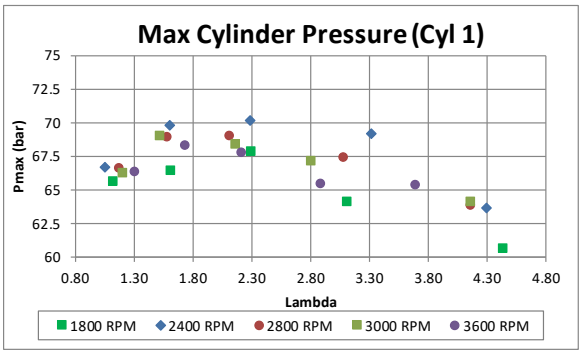

Figure 46: Phase 0 Pmax (cyl 1)

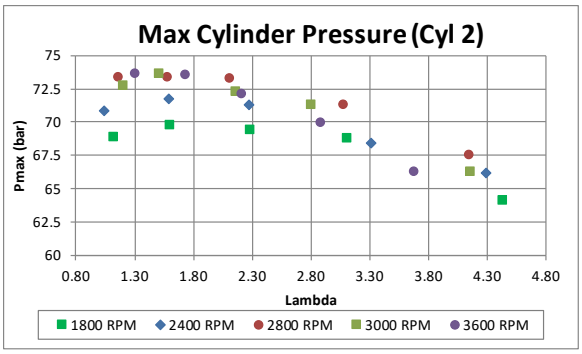

Figure 47: Phase 0 Pmax (cyl 2)

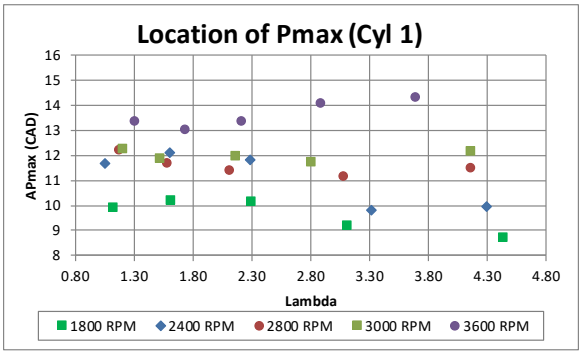

Figure 48: Phase 0 Pmax location (cyl 1)

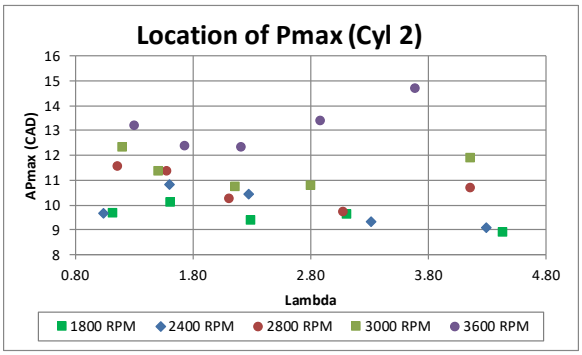

Figure 49: Phase 0 Pmax location (cyl 2)

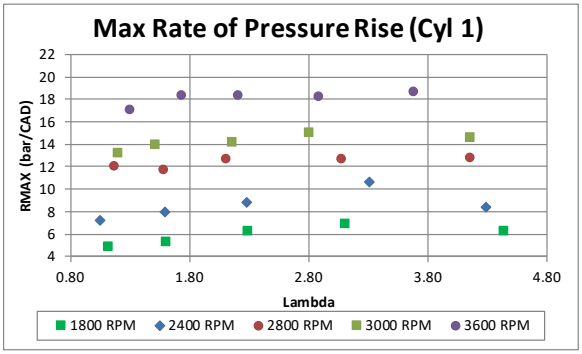

Figure 50: Phase 0 Pmax rise (cyl 1)

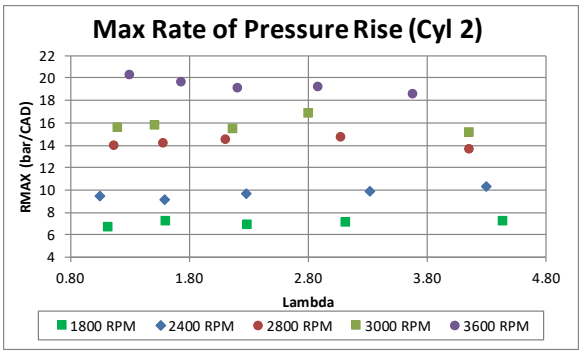

Figure 51: Phase 0 Pmax rise (cyl 2)

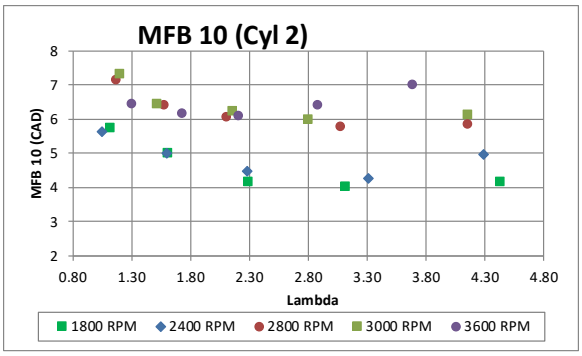

Figure 55: Phase 0 MFB 10 (cyl 2)

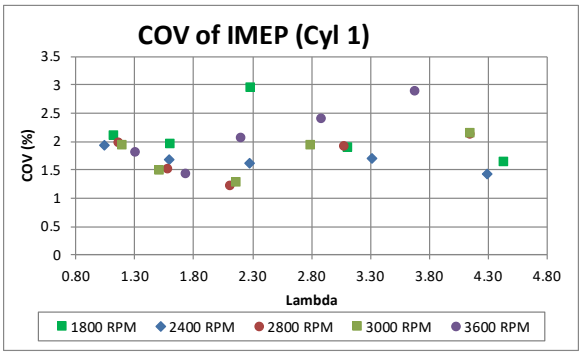

Figure 52: Phase 0 COV of IMEP (cyl 1)

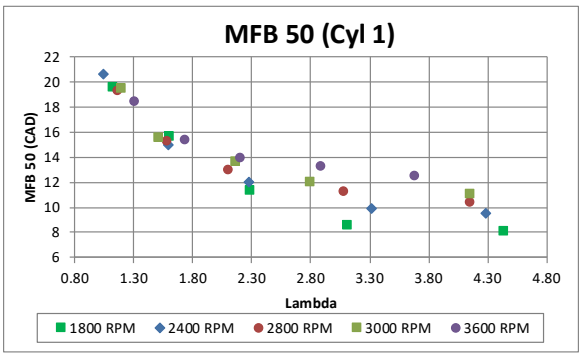

Figure 56: Phase 0 MFB 50 (cyl 1)

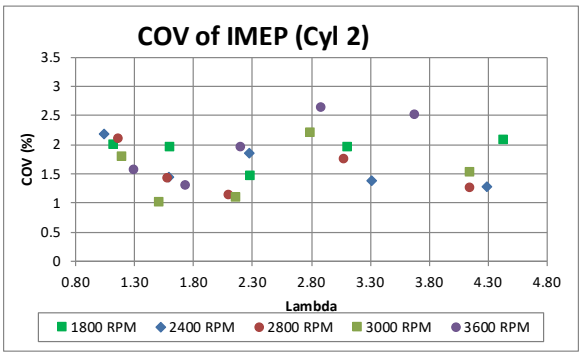

Figure 53: Phase 0 COV of IMEP (cyl 2)

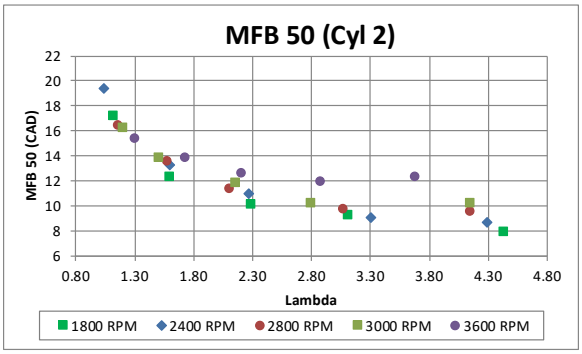

Figure 57: Phase 0 MFB 50 (cyl 2)

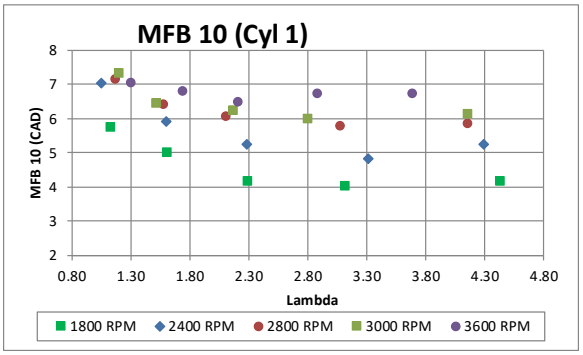

Figure 54: Phase 0 MFB 10 (cyl 1)

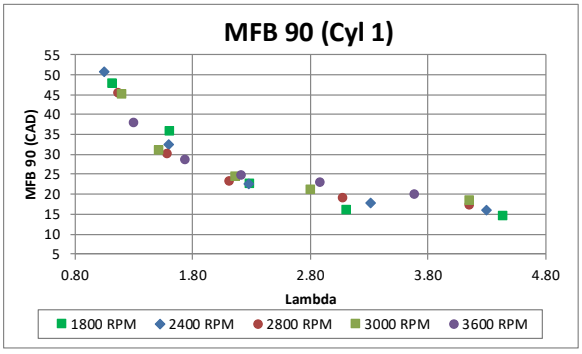

Figure 58: Phase 0 MFB 90 (cyl 1)

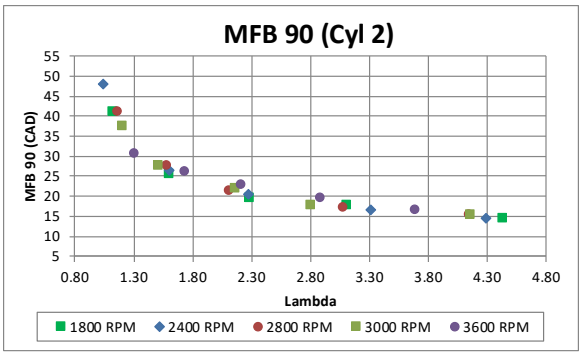

Figure 59: Phase 0 MFB 90 (cyl 2)

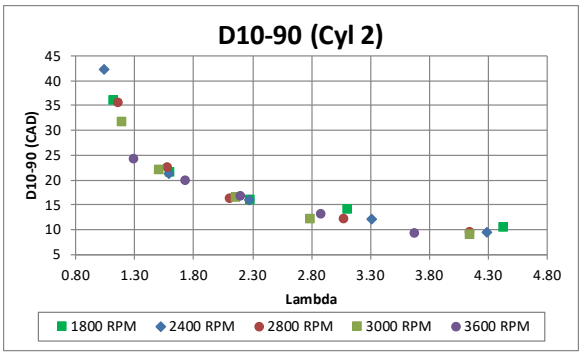

Figure 61: Phase 0 D10-90 (cyl 2)

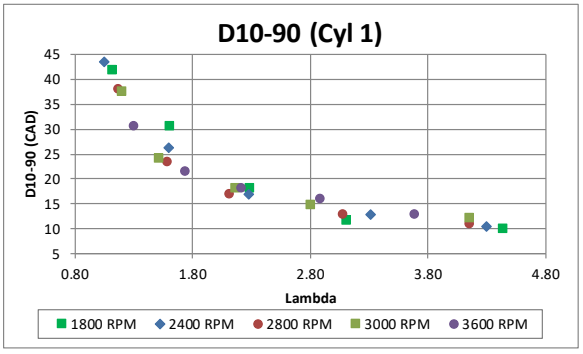

Figure 60: Phase 0 D10-90 (cyl 1)

Appendix 4: Phase 1.1 – Fueling Adjustment

Dyno Data

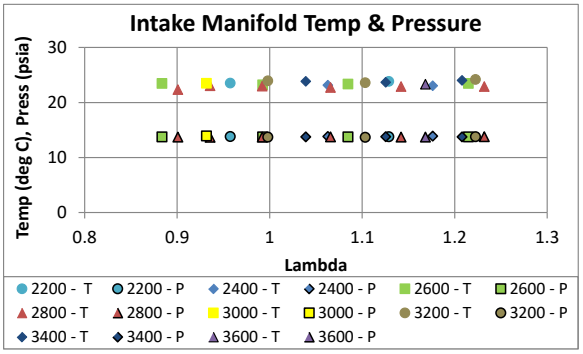

Figure 62: Phase 1.1 T_{intk_mnfld} & P_{intk_mnfld}

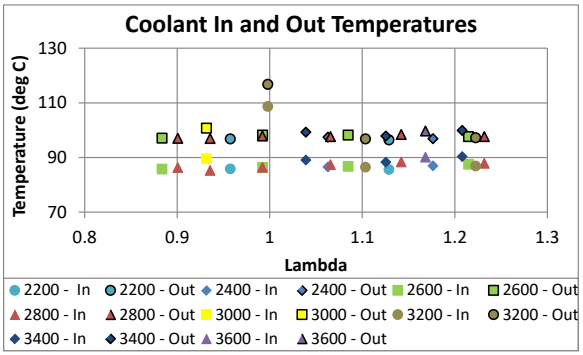

Figure 63: Phase 1.1 coolant temperatures

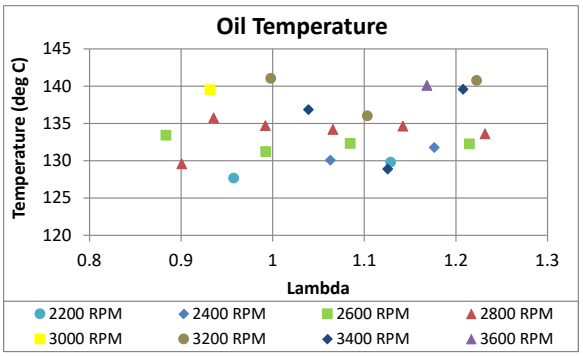

Figure 64: Phase 1.1 oil temperature

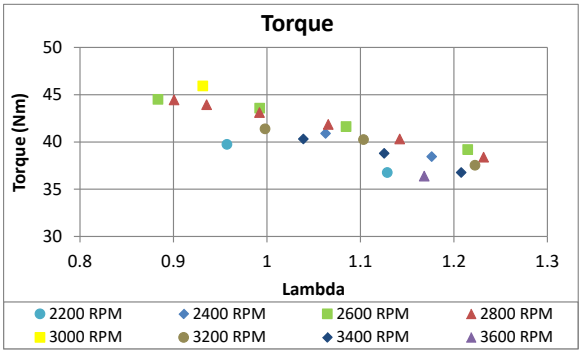

Figure 65: Phase 1.1 brake torque

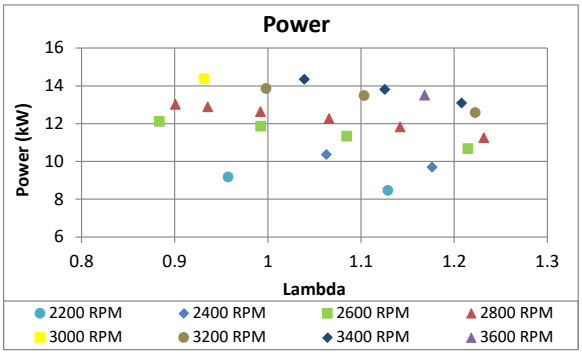

Figure 66: Phase 1.1 brake power

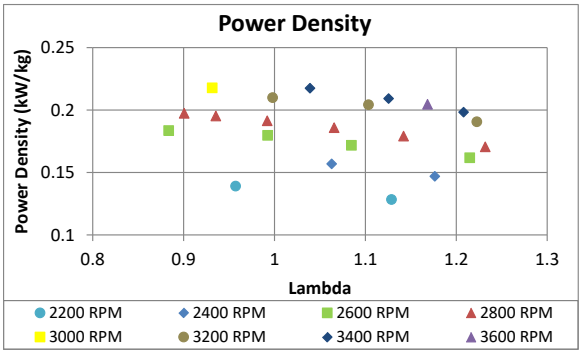

Figure 67: Phase 1.1 power density

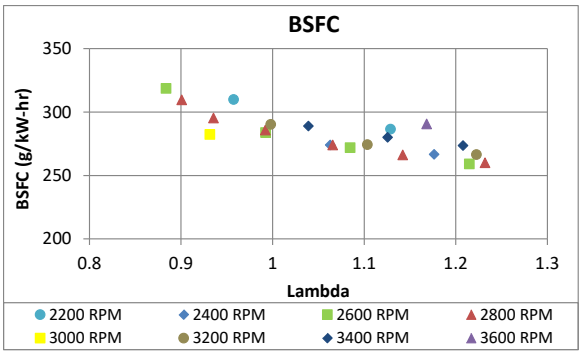

Figure 68: Phase 1.1 BSFC

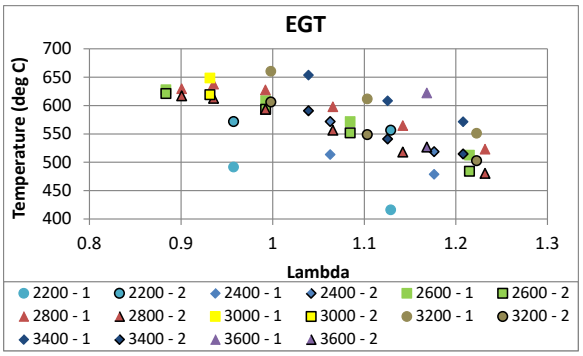

Figure 69: Phase 1.1 EGT

Fuel Energy Distribution Data

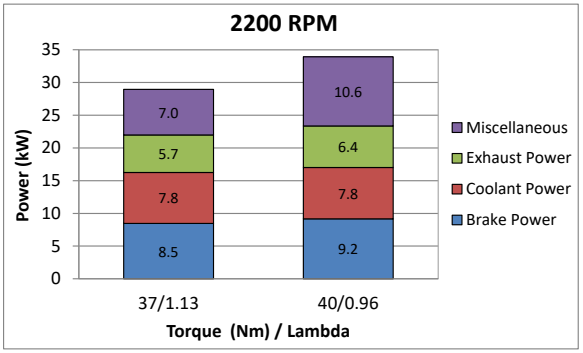

Figure 70: Phase 1.1 energy distribution @ 2200 RPM

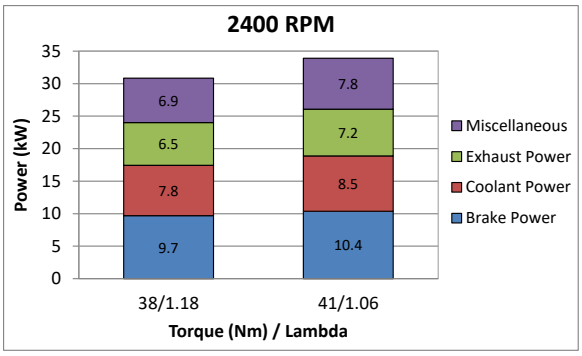

Figure 71: Phase 1.1 energy distribution @ 2400 RPM

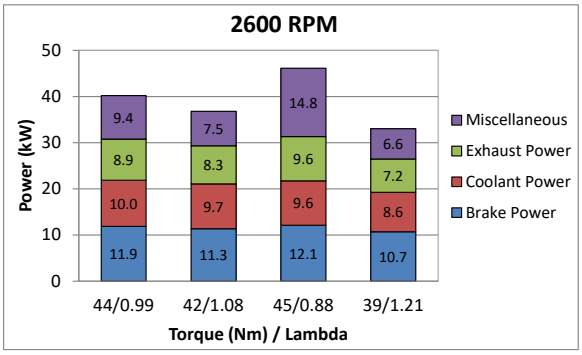

Figure 72: Phase 1.1 energy distribution @ 2600 RPM

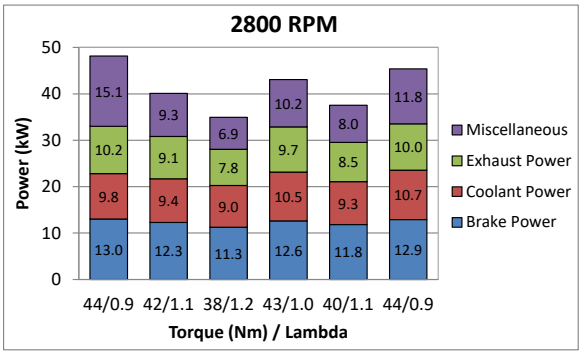

Figure 73: Phase 1.1 energy distribution @ 2800 RPM

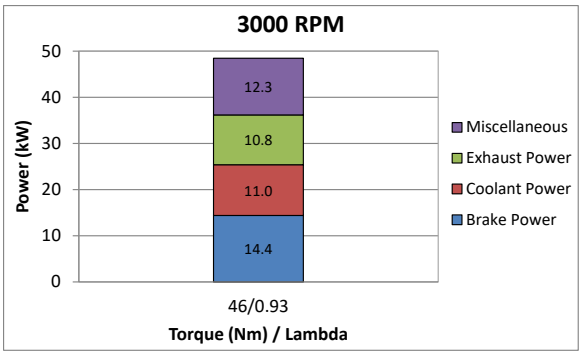

Figure 74: Phase 1.1 energy distribution @ 3000 RPM

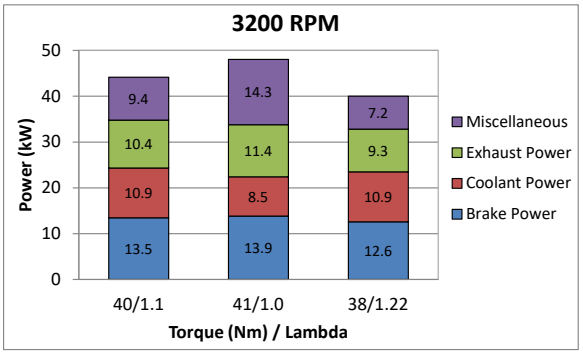

Figure 75: Phase 1.1 energy distribution @ 3200 RPM

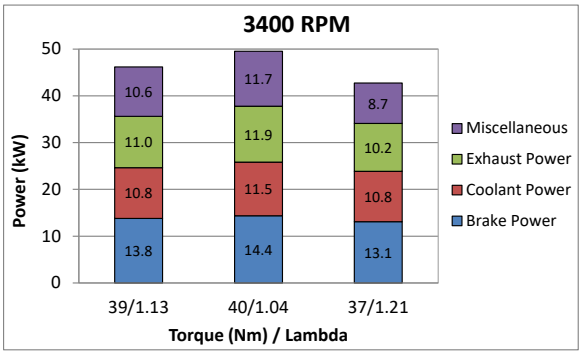

Figure 76: Phase 1.1 energy distribution @ 3400 RPM

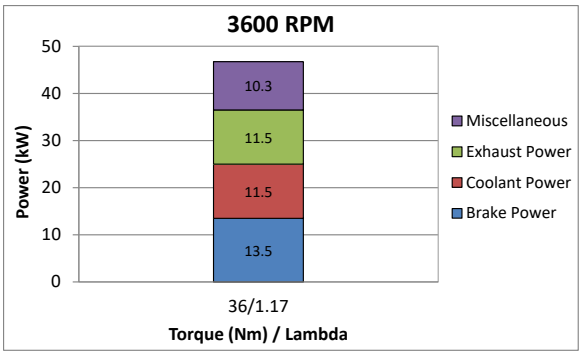

Figure 77: Phase 1.1 energy distribution @ 3600 RPM

Smoke Data

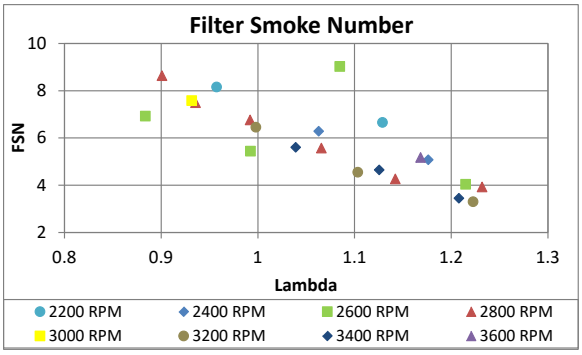

Figure 78: Phase 1.1 filter smoke number

Combustion Data

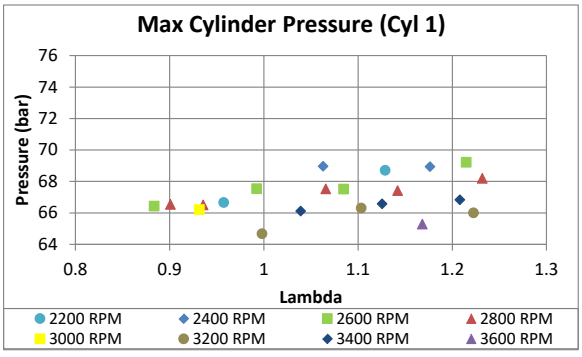

Figure 79: Phase 1.1 Pmax (cyl 1)

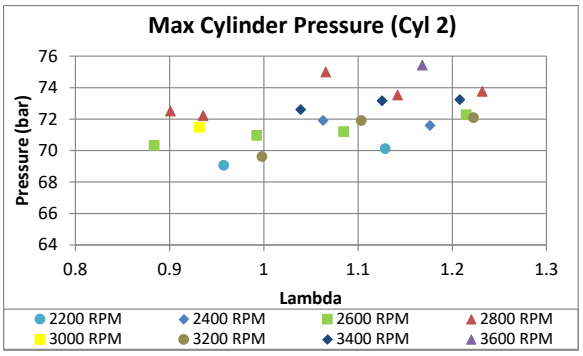

Figure 80: Phase 1.1 Pmax (cyl 2)

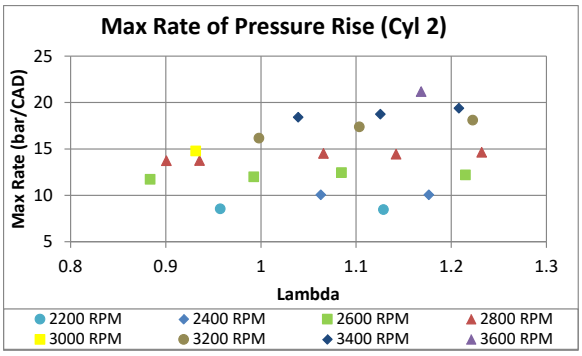

Figure 84: Phase 1.1 Pmax rise (cyl 2)

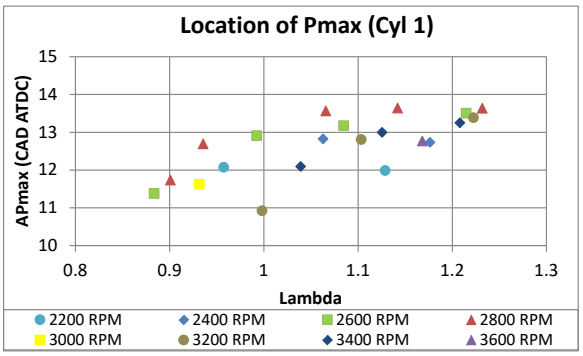

Figure 81: Phase 1.1 Pmax location (cyl 1)

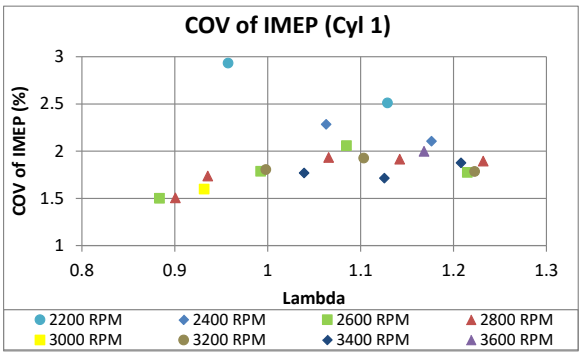

Figure 85: Phase 1.1 COV of IMEP (cyl 1)

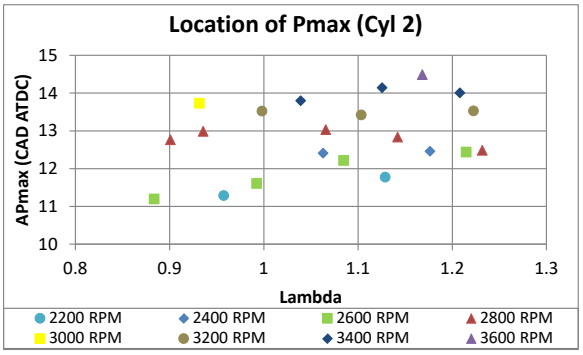

Figure 82: Phase 1.1 Pmax location (cyl 2)

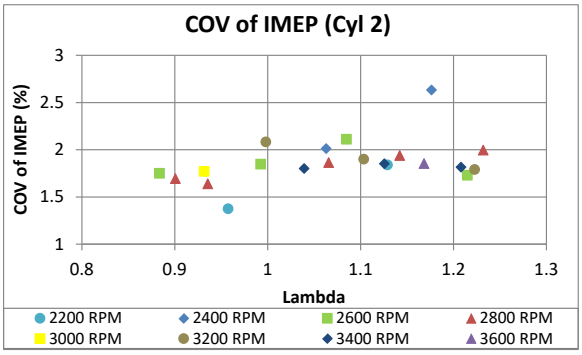

Figure 86: Phase 1.1 COV of IMEP (cyl 2)

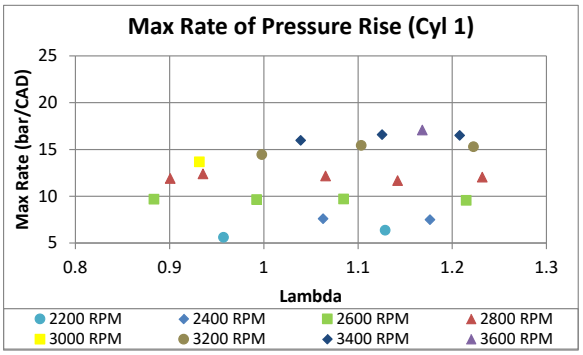

Figure 83: Phase 1.1 Pmax rise (cyl 1)

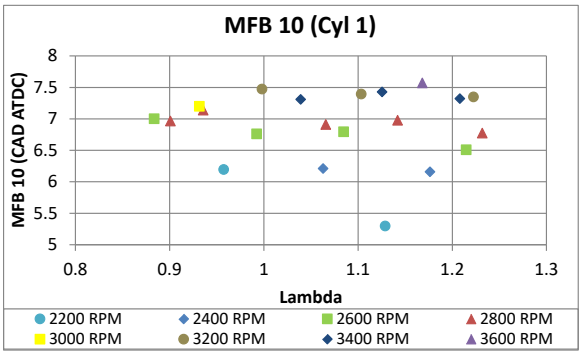

Figure 87: Phase 1.1 MFB 10 (cyl 1)

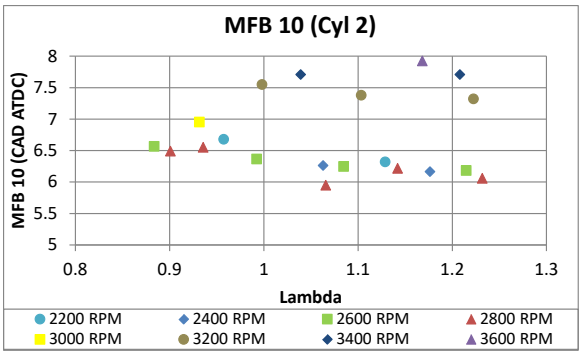

Figure 88: Phase 1.1 MFB 10 (cyl 2)

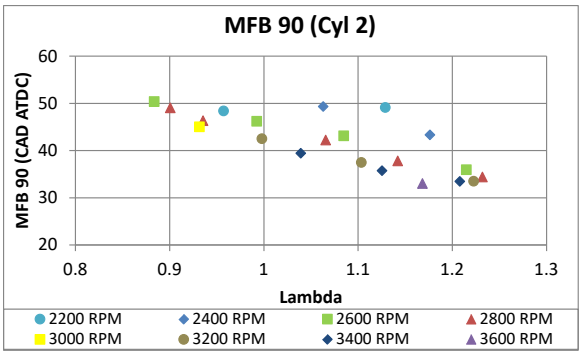

Figure 92: Phase 1.1 MFB 90 (cyl 2)

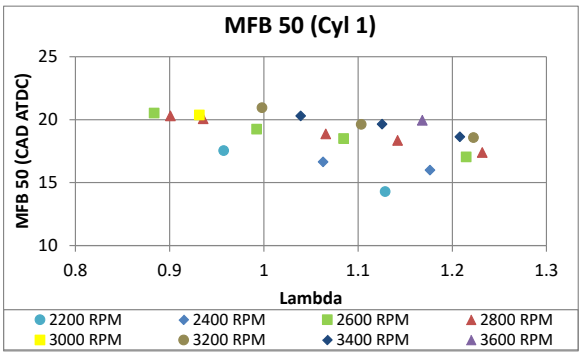

Figure 89: Phase 1.1 MFB 50 (cyl 1)

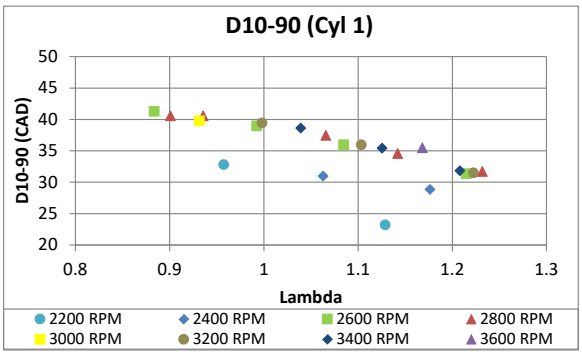

Figure 93: Phase 1.1 D10-90 (cyl 1)

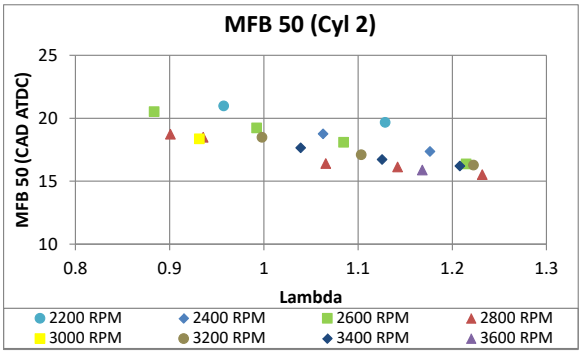

Figure 90: Phase 1.1 MFB 50 (cyl 2)

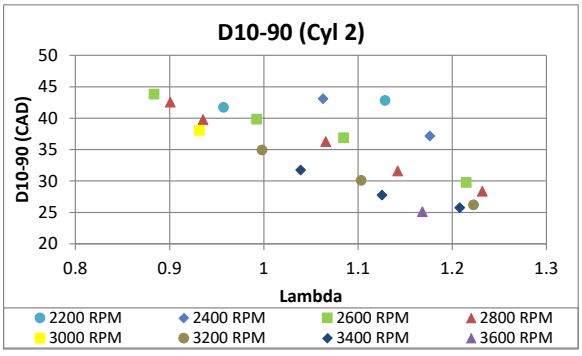

Figure 94: Phase 1.1 D10-90 (cyl 2)

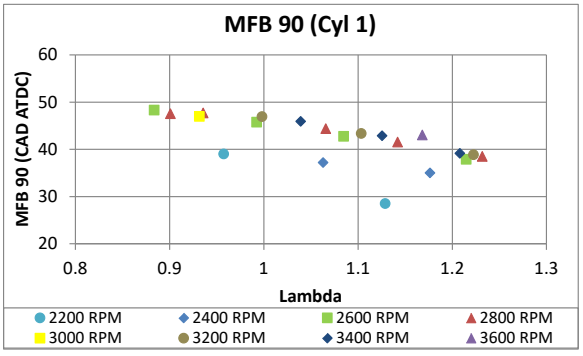

Figure 91: Phase 1.1 MFB 90 (cyl 1)

Appendix 5: Phase 1.2 – Injector Advance

Dyno Data

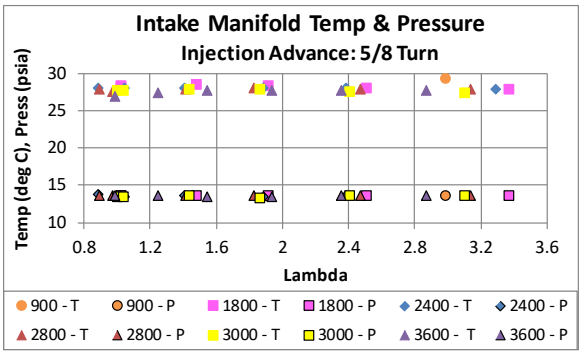

Figure 95: Phase 1.2 T_{intk_mnfld} & P_{intk_mnfld}

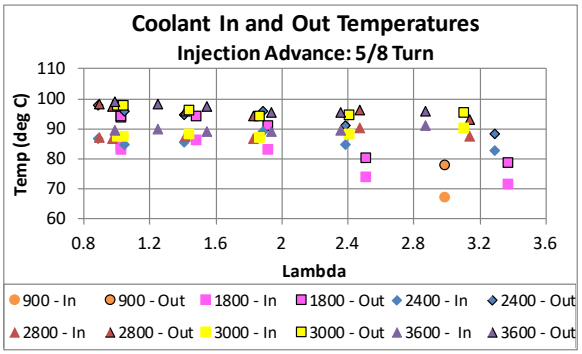

Figure 96: Phase 1.2 coolant temperatures

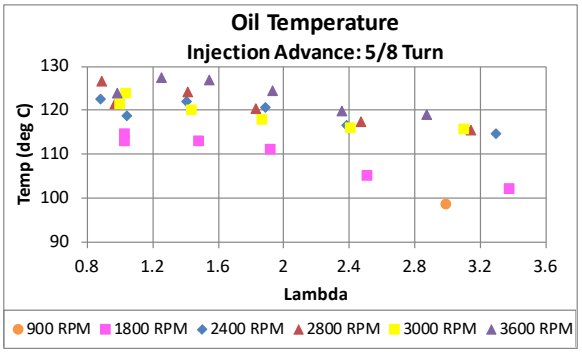

Figure 97: Phase 1.2 oil temperature

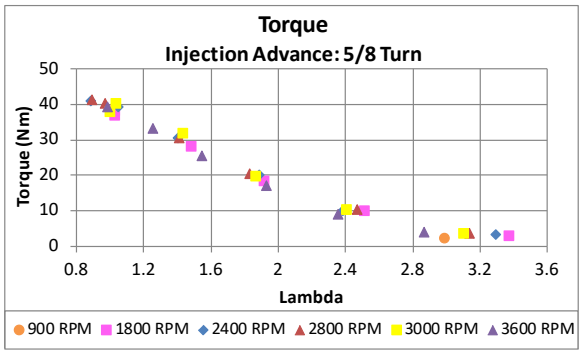

Figure 98: Phase 1.2 brake torque

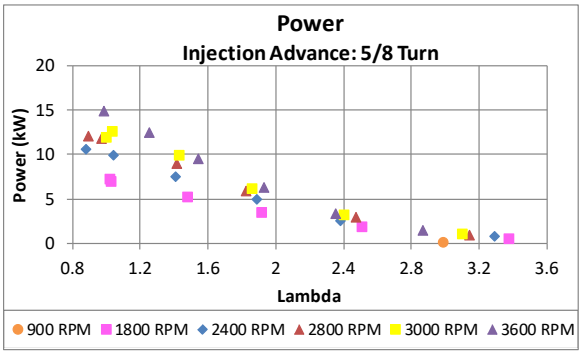

Figure 99: Phase 1.2 brake power

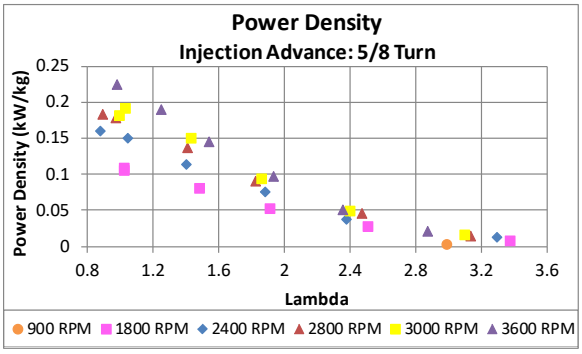

Figure 100: Phase 1.2 power density

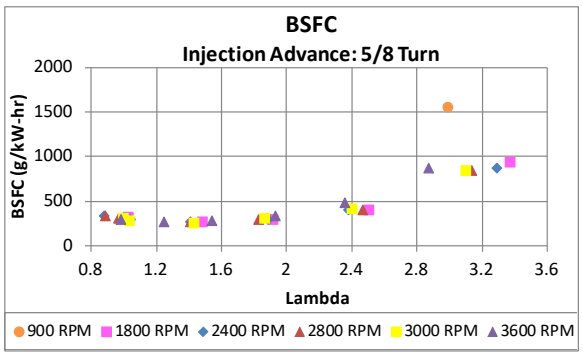

Figure 101: Phase 1.2 BSFC

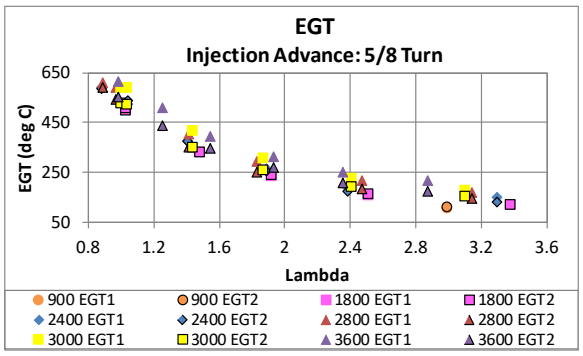

Figure 102: Phase 1.2: EGT

Fuel Energy Distribution Data

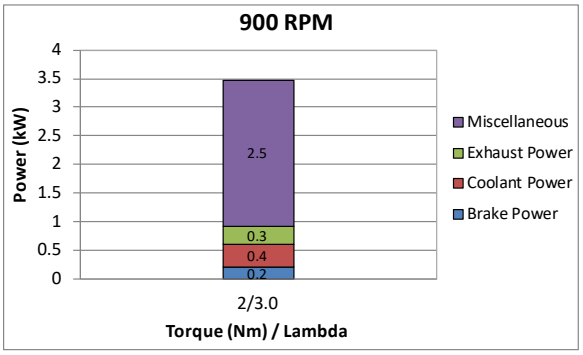

Figure 103: Phase 1.2 energy distribution @ 900 RPM

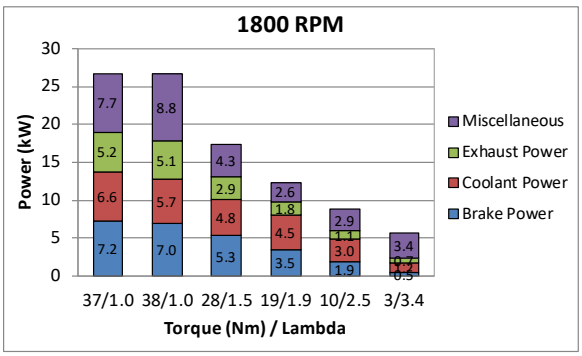

Figure 104: Phase 1.2 energy distribution @ 1800 RPM

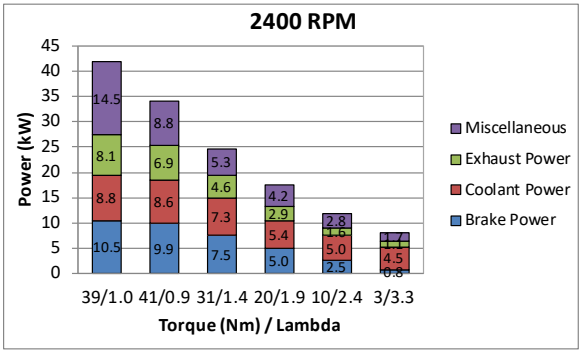

Figure 105: Phase 1.2 energy distribution @ 2400 RPM

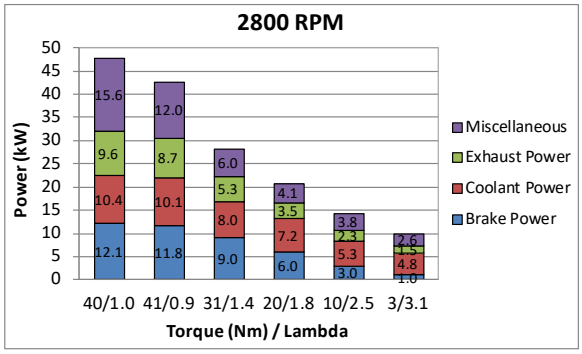

Figure 106: Phase 1.2 energy distribution @ 2800 RPM

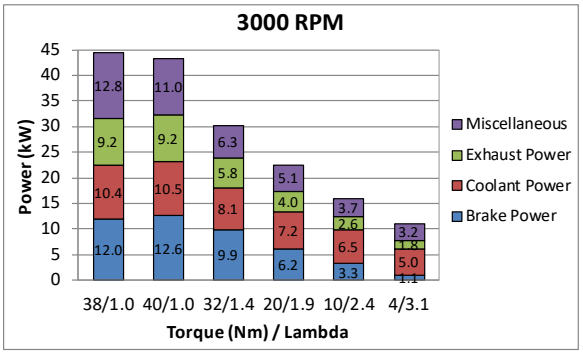

Figure 107: Phase 1.2 energy distribution @ 3000 RPM

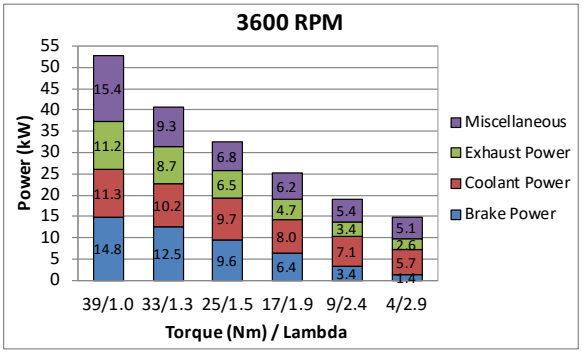

Figure 108: Phase 1.2 energy distribution @ 3600 RPM

Smoke Data

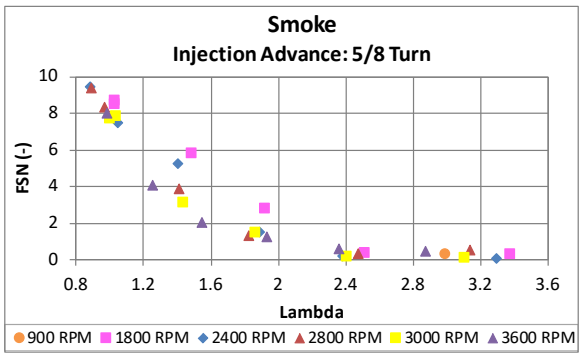

Figure 109: Phase 1.2 filter smoke number

Combustion Data

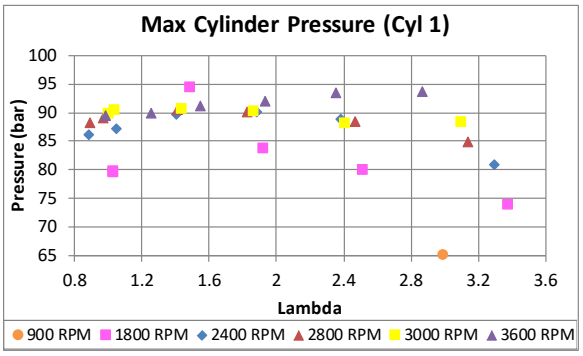

Figure 110: Phase 1.2 Pmax (cyl 1)

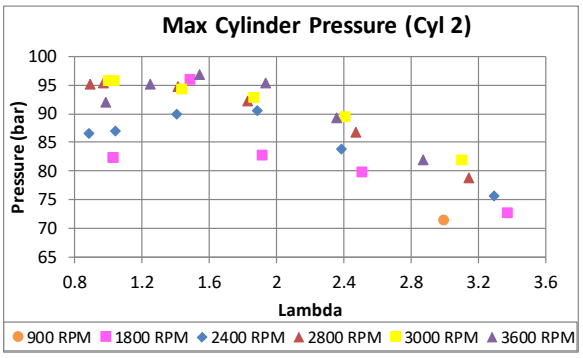

Figure 111: Phase 1.2 Pmax (cyl 2)

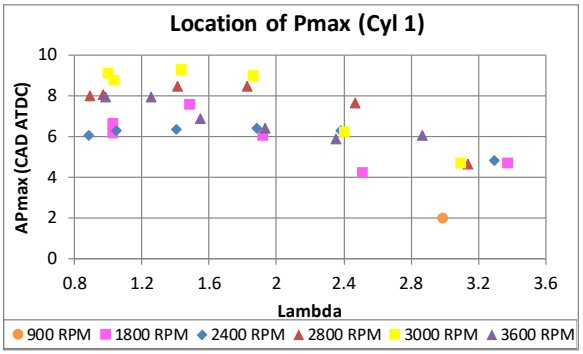

Figure 112: Phase 1.2 Pmax location (cyl 1)

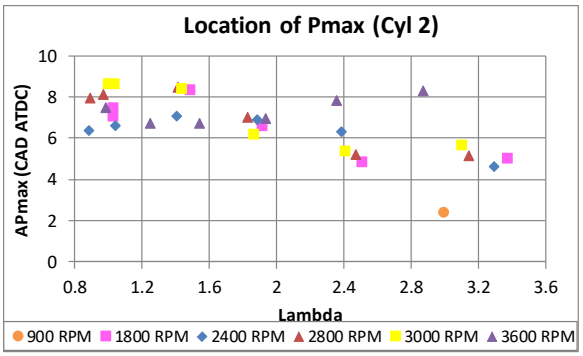

Figure 113: Phase 1.2 Pmax location (cyl 2)

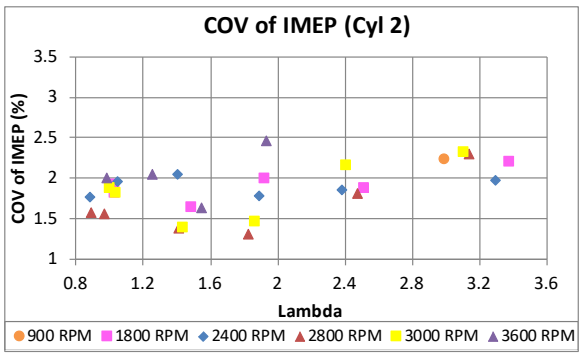

Figure 117: Phase 1.2 COV of IMEP (cyl 2)

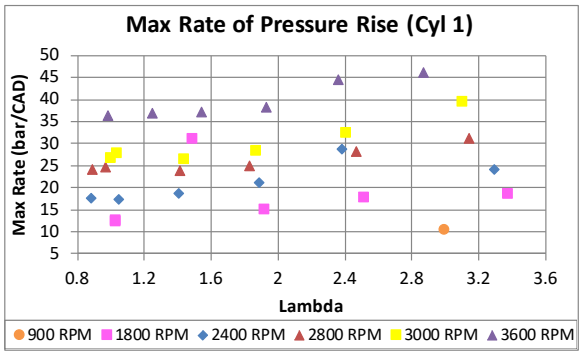

Figure 114: Phase 1.2 Pmax rise (cyl 1)

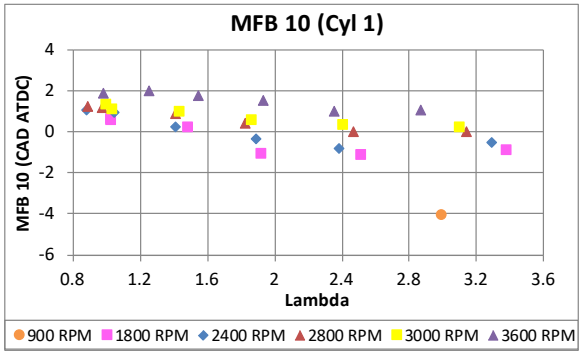

Figure 118: Phase 1.2 MFB 10 (cyl 1)

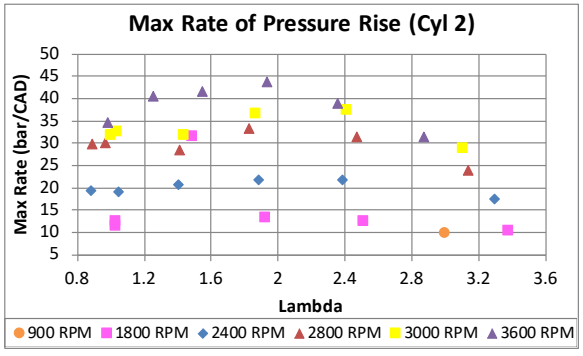

Figure 115: Phase 1.2 Pmax rise (cyl 2)

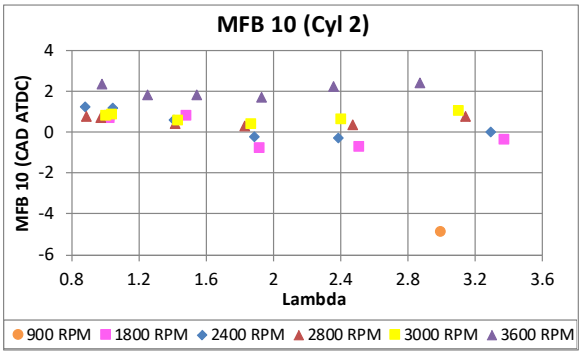

Figure 119: Phase 1.2 MFB 10 (cyl 2)

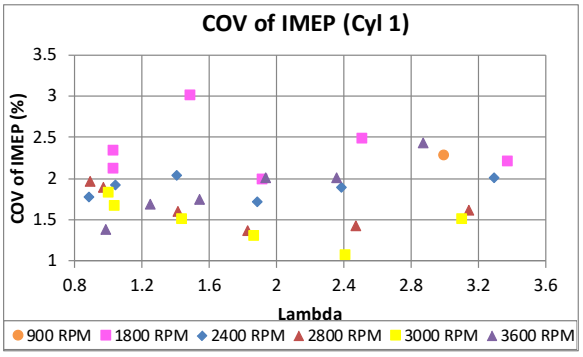

Figure 116: Phase 1.2 COV of IMEP (cyl 1)

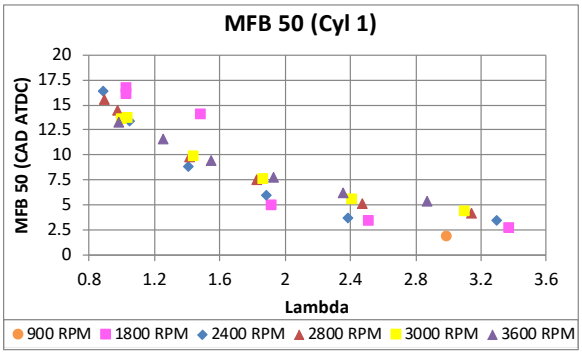

Figure 120: Phase 1.2 MFB 50 (cyl 1)

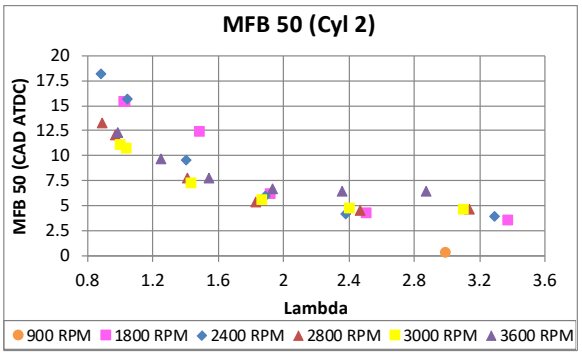

Figure 121: Phase 1.2 MFB 50 (cyl 2)

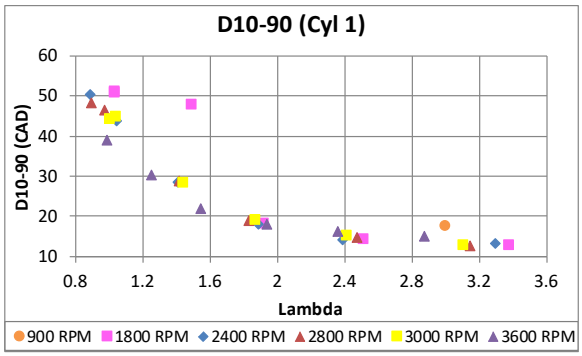

Figure 124: Phase 1.2 D10-90 (cyl 1)

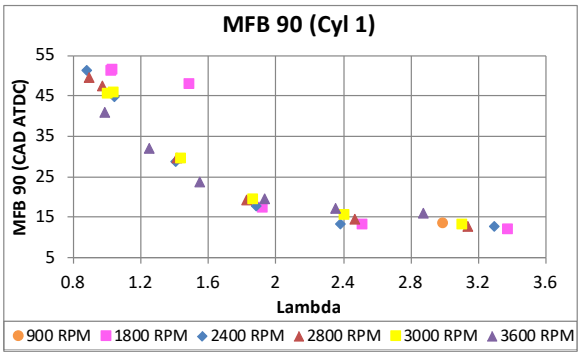

Figure 122: Phase 1.2 MFB 90 (cyl 1)

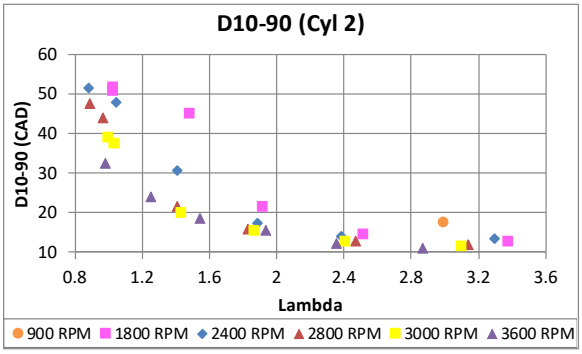

Figure 125: Phase 1.2 D10-90 (cyl 2)

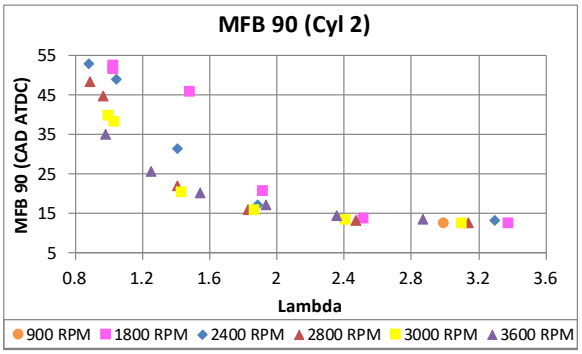

Figure 123: Phase 1.2 MFB 90 (cyl 2)

Appendix 6: Phase 1.3 – Volumetric Efficiency

Dyno Data

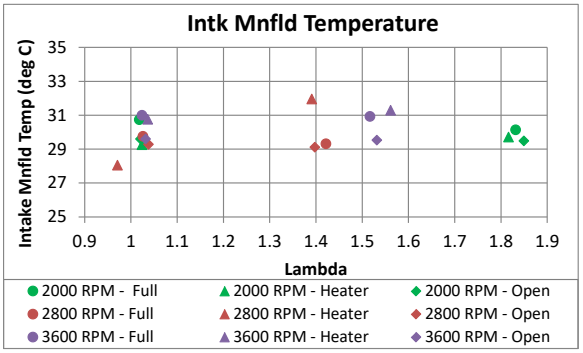

Figure 126: Phase 1.3 T_{intk_mnfld} & P_{intk_mnfld}

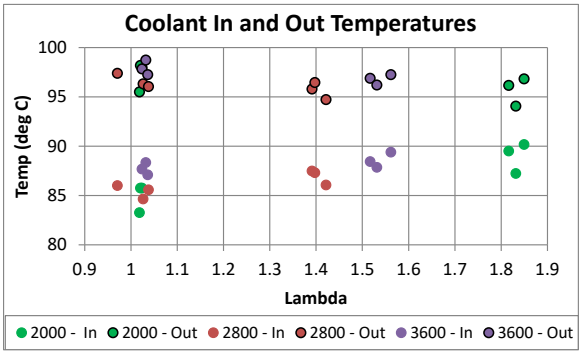

Figure 127: Phase 1.3 coolant temperatures

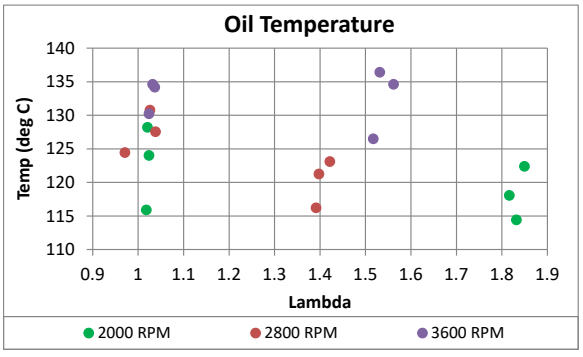

Figure 128: Phase 1.3 oil temperature

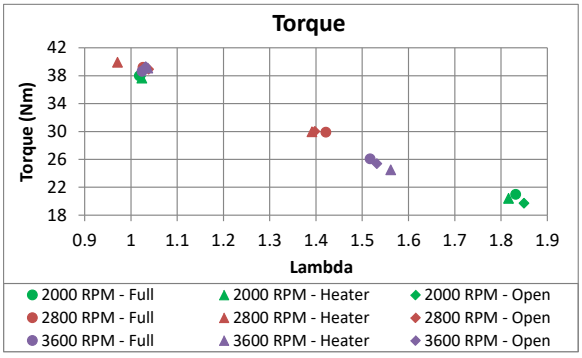

Figure 129: Phase 1.3 brake torque

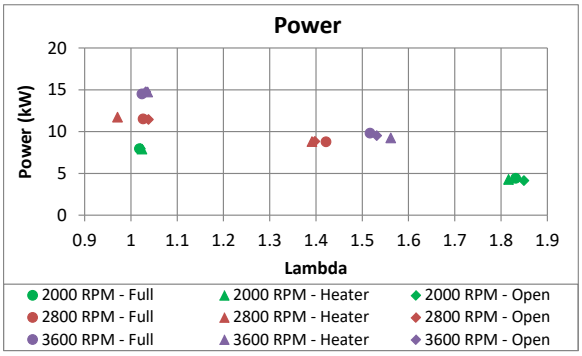

Figure 130: Phase 1.3 brake power

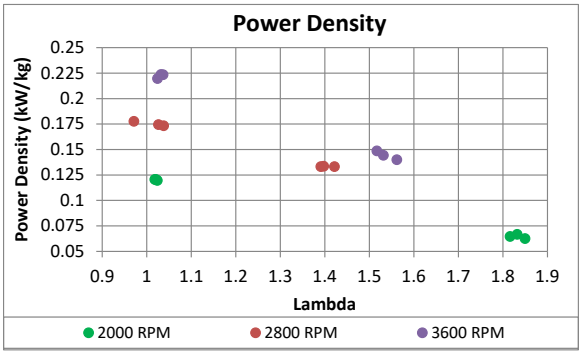

Figure 131: Phase 1.3 power density

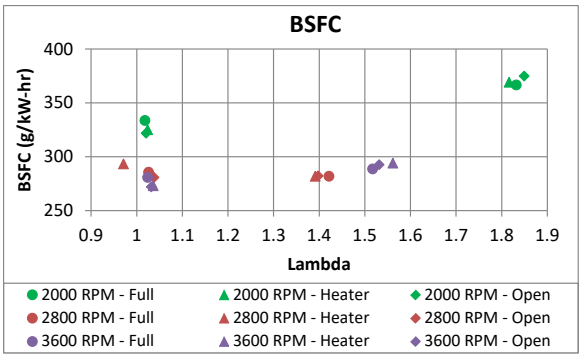

Figure 132: Phase 1.3 BSFC

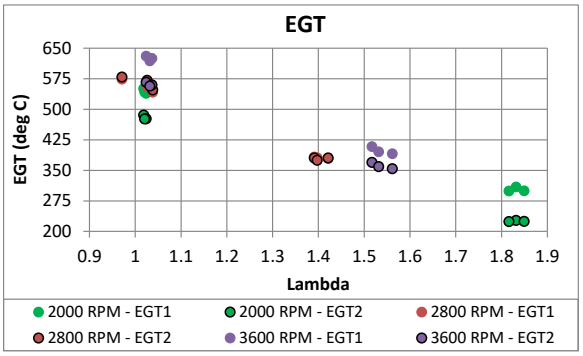

Figure 133: Phase 1.3 EGT

Fuel Energy Distribution Data

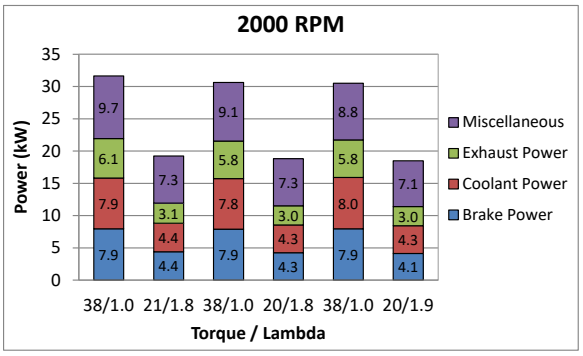

Figure 134: Phase 1.3 energy distribution @ 2000 RPM

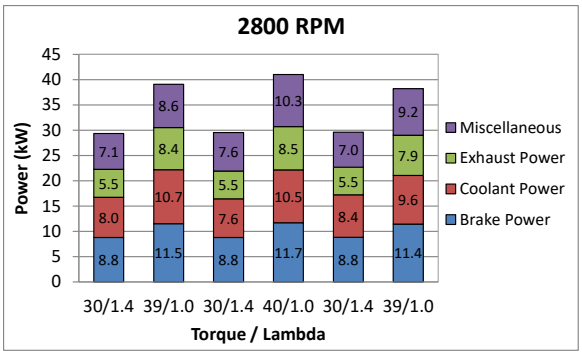

Figure 135: Phase 1.3 energy distribution @ 2800 RPM

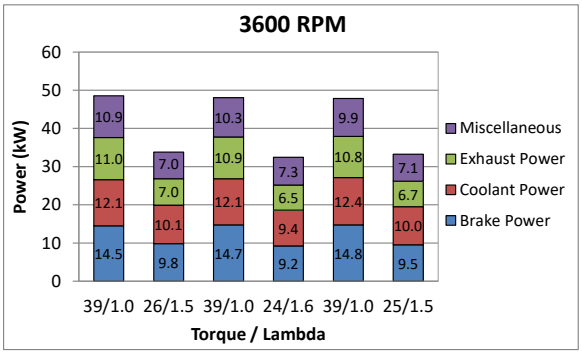

Figure 136: Phase 1.3 energy distribution @ 3600 RPM

Smoke Data

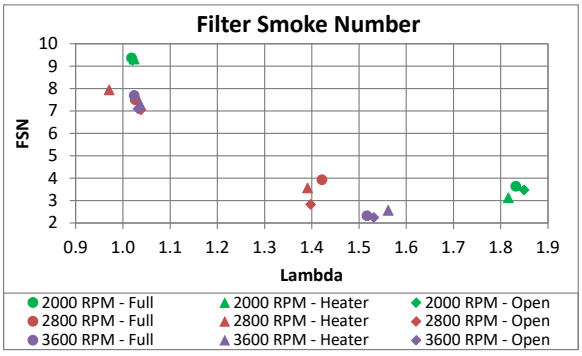

Figure 137: Phase 1.3 filter smoke number

Combustion Data

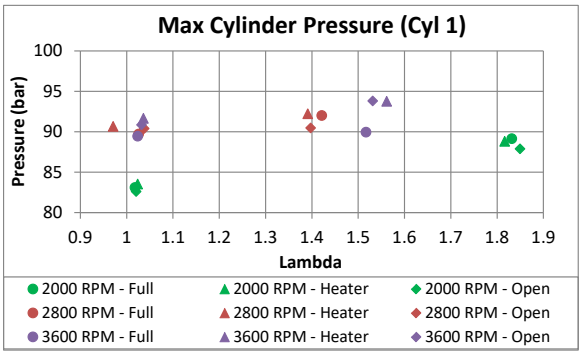

Figure 138: Phase 1.3 Pmax (cyl 1)

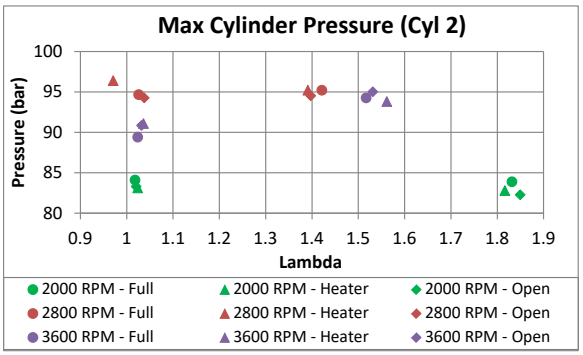

Figure 139: Phase 1.3 Pmax (cyl 2)

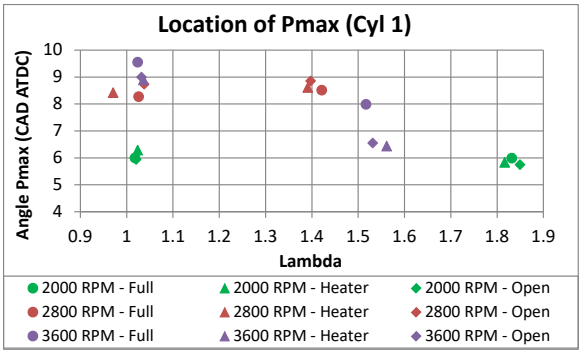

Figure 140: Phase 1.3 Pmax location (cyl 1)

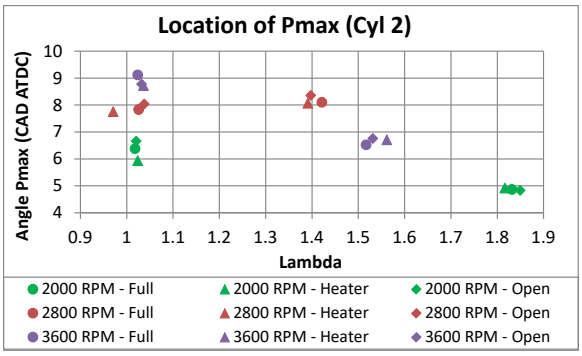

Figure 141: Phase 1.3 Pmax location (cyl 2)

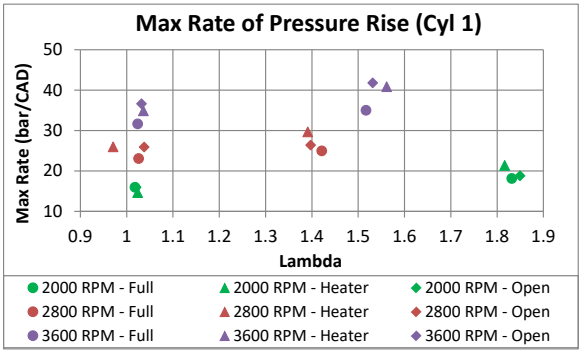

Figure 142: Phase 1.3 Pmax rise (cyl 1)

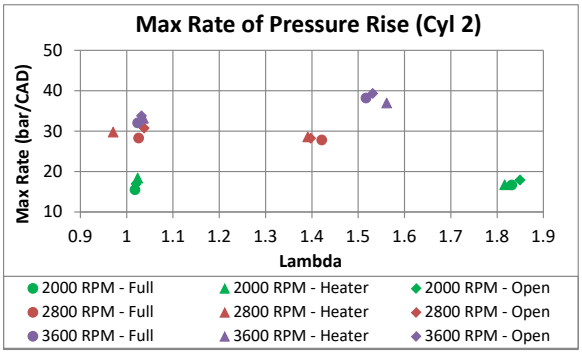

Figure 143: Phase 1.3 Pmax rise (cyl 2)

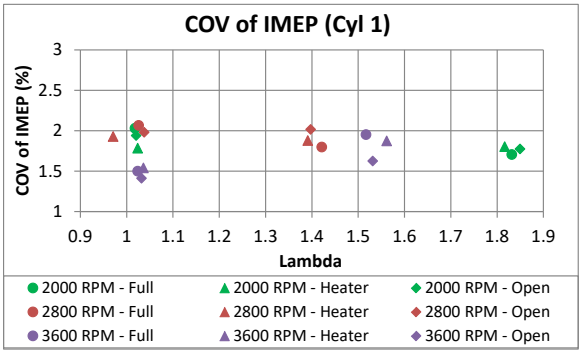

Figure 144: Phase 1.3 COV of IMEP (cyl 1)

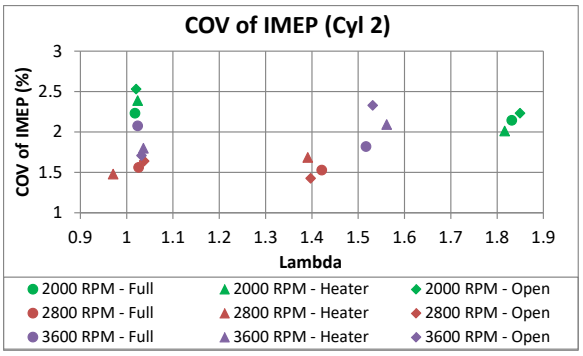

Figure 145: Phase 1.3 COV of IMEP (cyl 2)

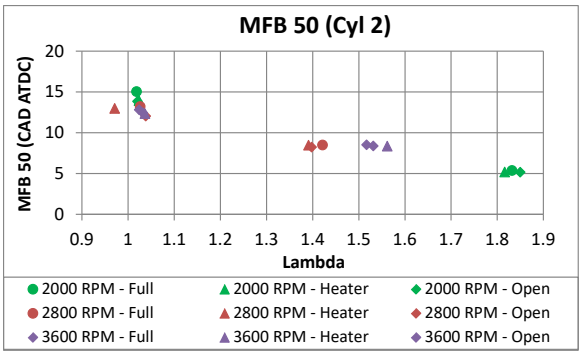

Figure 149: Phase 1.3 MFB 50 (cyl 2)

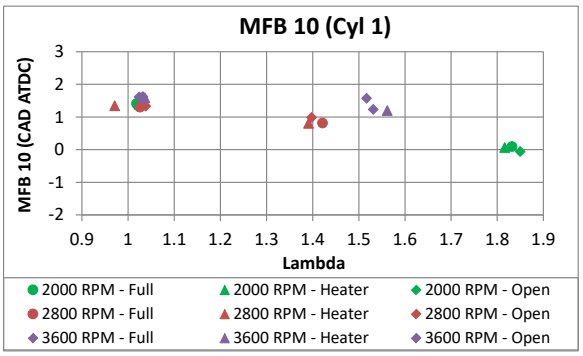

Figure 146: Phase 1.3 MFB 10 (cyl 1)

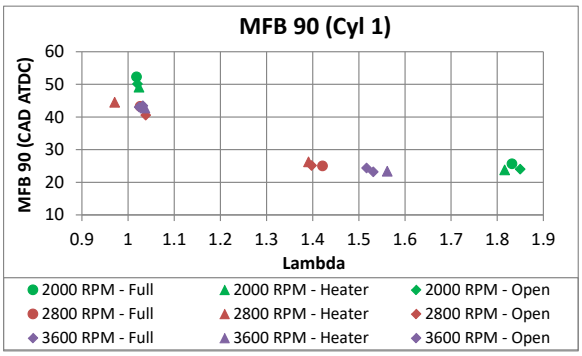

Figure 150: Phase 1.3 MFB 90 (cyl 1)

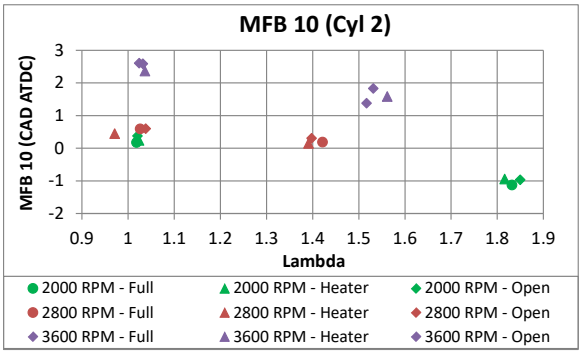

Figure 147: Phase 1.3 MFB 10 (cyl 2)

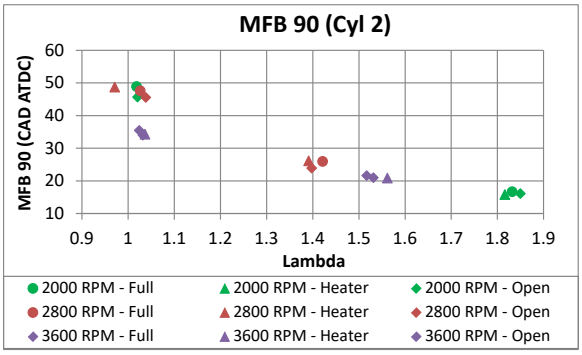

Figure 151: Phase 1.3 MFB 90 (cyl 2)

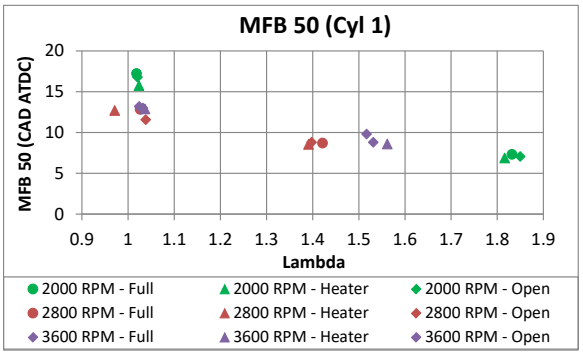

Figure 148: Phase 1.3 MFB 50 (cyl 1)

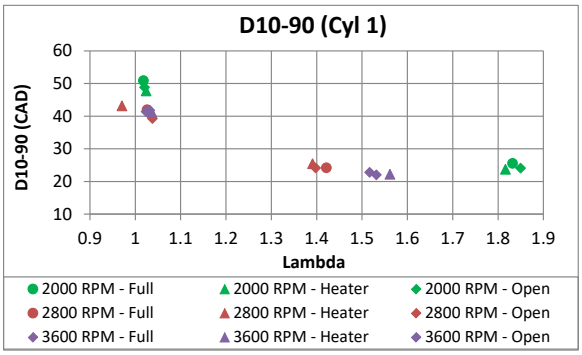

Figure 152: Phase 1.3 D10-90 (cyl 1)

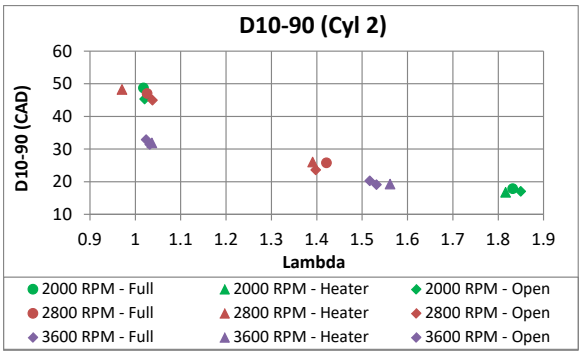

Figure 153: Phase 1.3 D10-90 (cyl 2)

Appendix 7: Phase 1.4 – F-24

Dyno Data

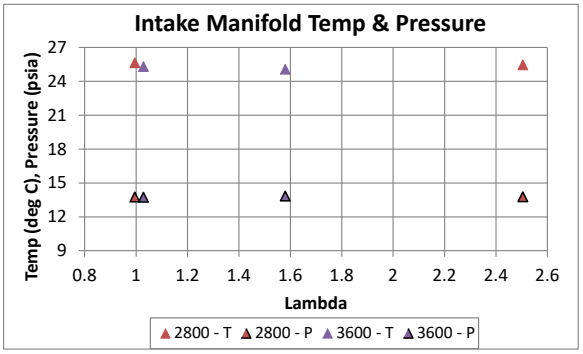

Figure 154: Phase 1.4 T_{intk_mnfld} & P_{intk_mnfld}

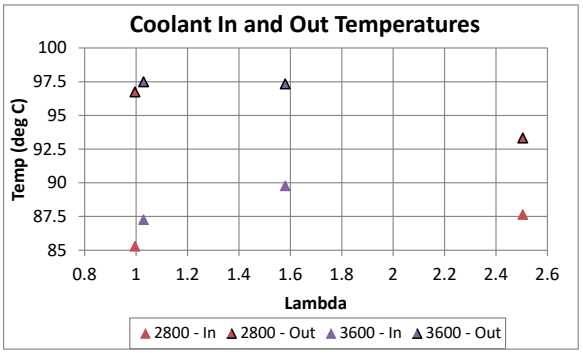

Figure 155: Phase 1.4 coolant temperatures

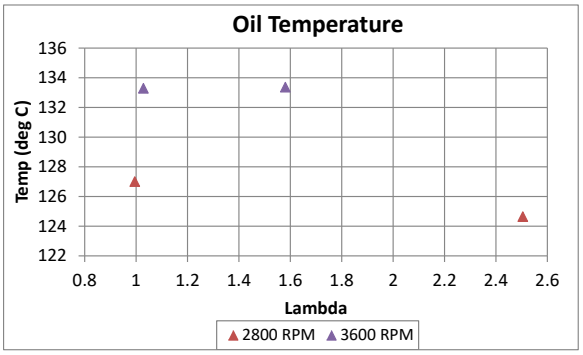

Figure 156: Phase 1.4: oil temperature

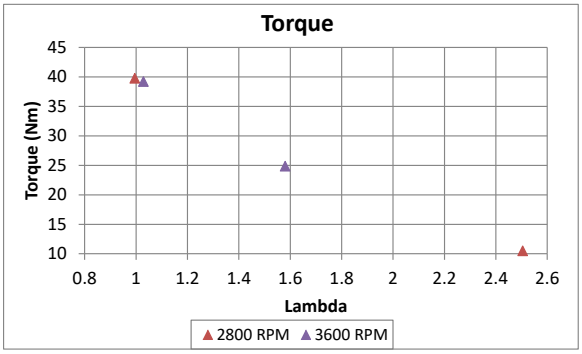

Figure 157: Phase 1.4 brake torque

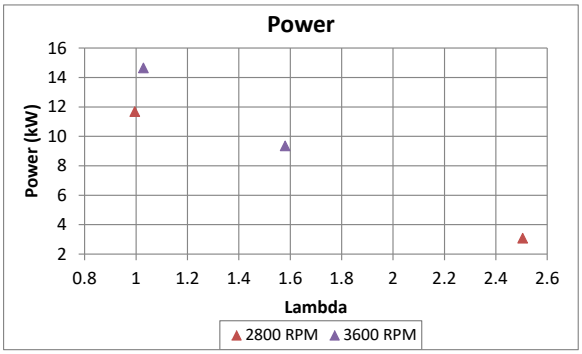

Figure 158: Phase 1.4: brake power

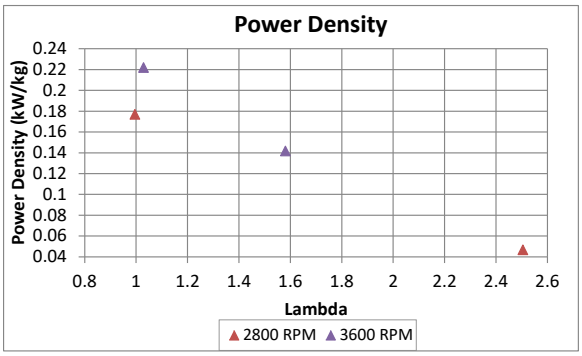

Figure 159: Phase 1.4: power density

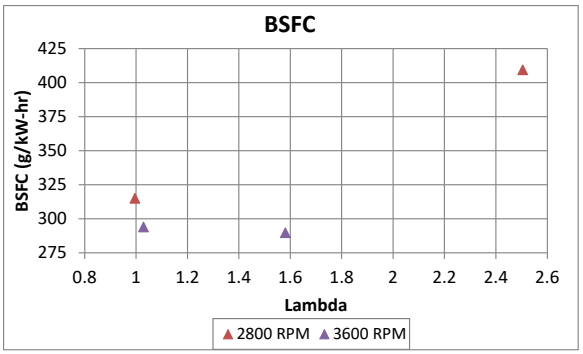

Figure 160: Phase 1.4: BSFC

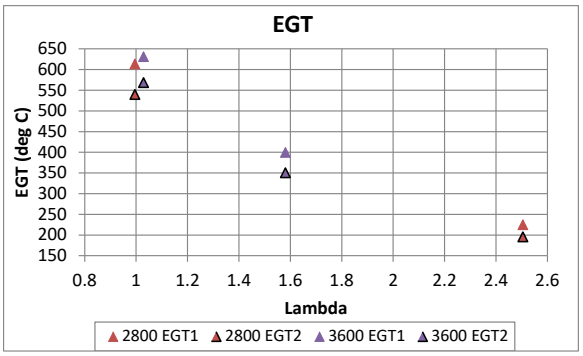

Figure 161: Phase 1.4: EGT

Fuel Energy Distribution Data

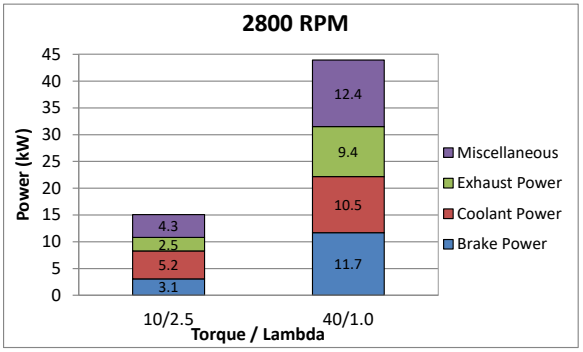

Figure 162: Phase 1.4 energy distribution @ 2800 RPM

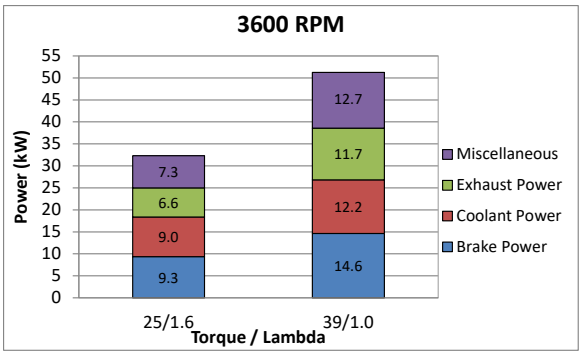

Figure 163: Phase 1.4 energy distribution @ 3600 RPM

Smoke Data

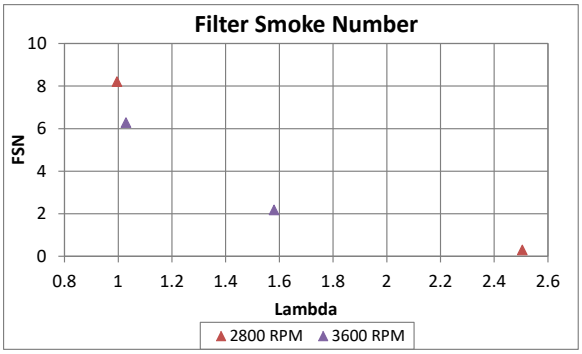

Figure 164: Phase 1.4 filter smoke number

Combustion Data

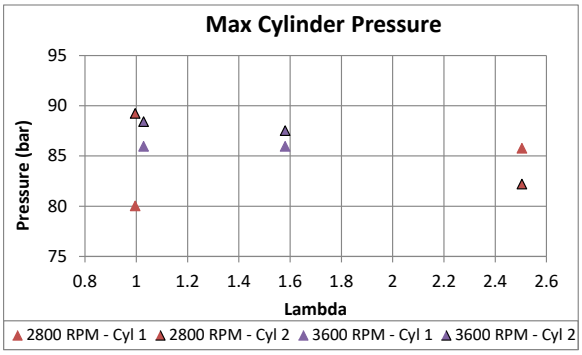

Figure 165: Phase 1.4 Pmax

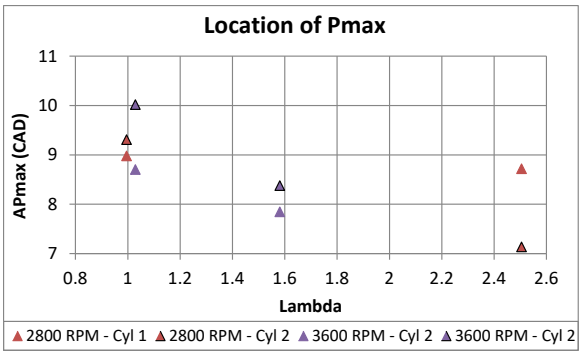

Figure 166: Phase 1.4 Pmax location

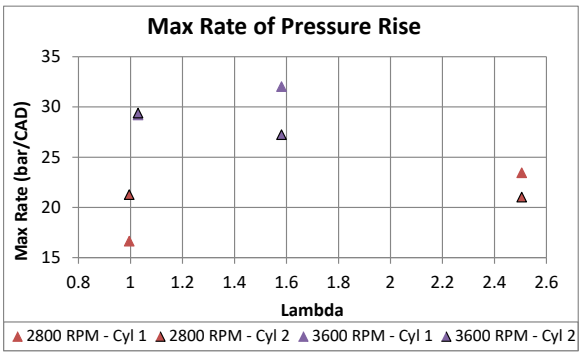

Figure 167: Phase 1.4 Pmax rise

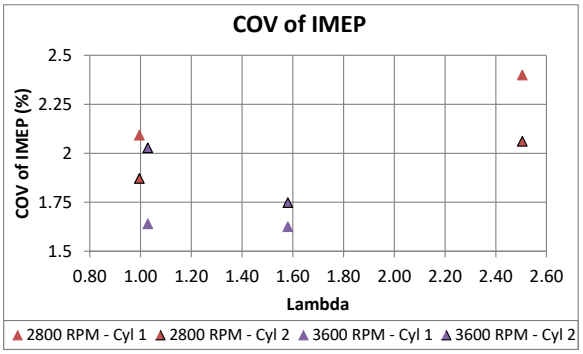

Figure 168: Phase 1.4 COV of IMEP

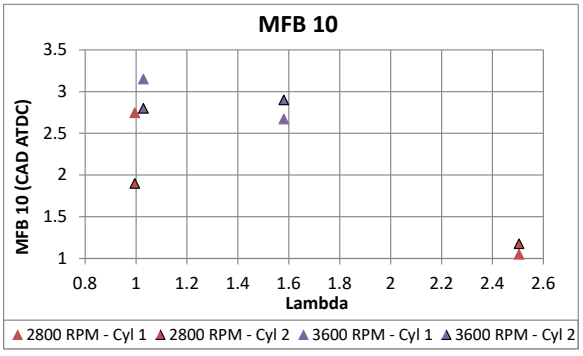

Figure 169: Phase 1.4 MFB 10

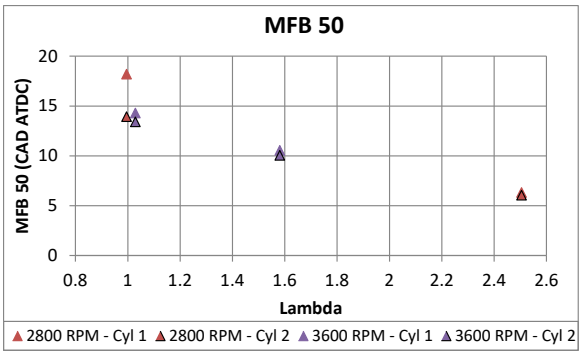

Figure 170: Phase 1.4 MFB 50

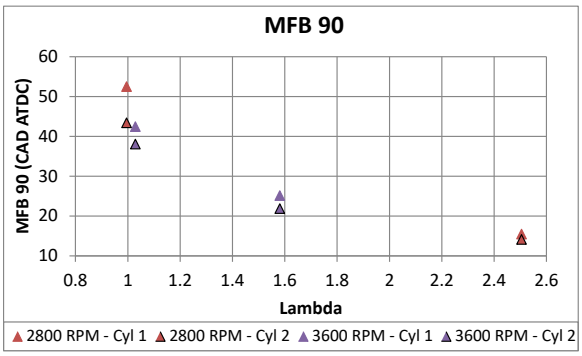

Figure 171: Phase 1.4 MFB 90

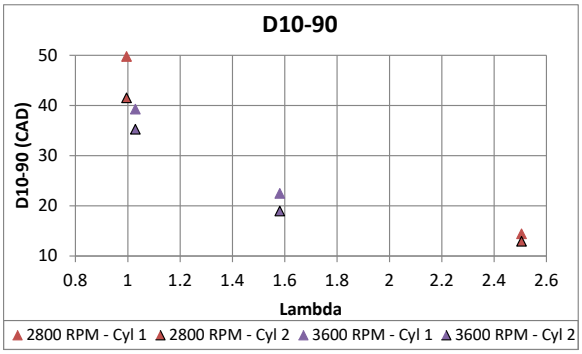

Figure 172: Phase 1.4 D10-90

Appendix 8: Phase 2 – Boost

Dyno Data

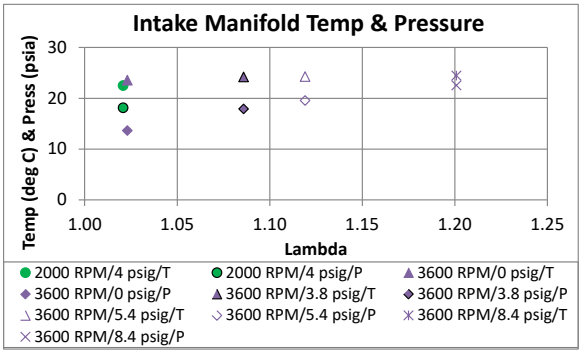

Figure 173: Phase 2 T_{intk_mnfld} & P_{intk_mnfld}

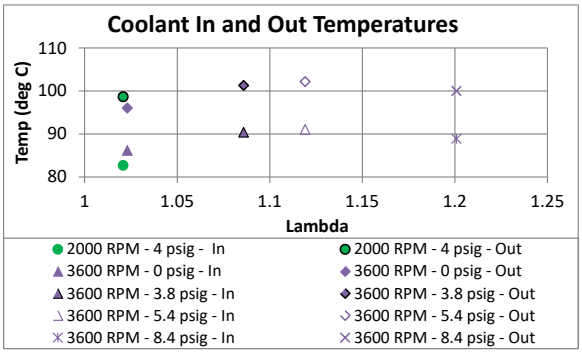

Figure 174: Phase 2 coolant temperatures

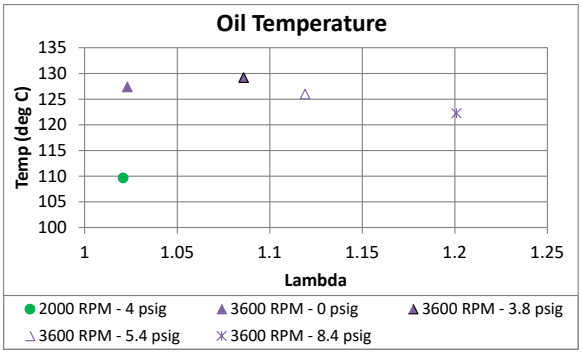

Figure 175: Phase 2 oil temperature

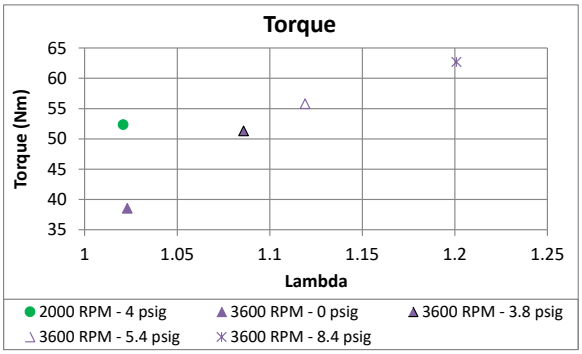

Figure 176: Phase 2 brake torque

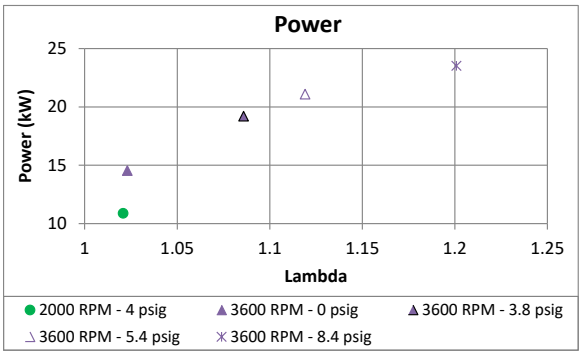

Figure 177: Phase 2 brake power

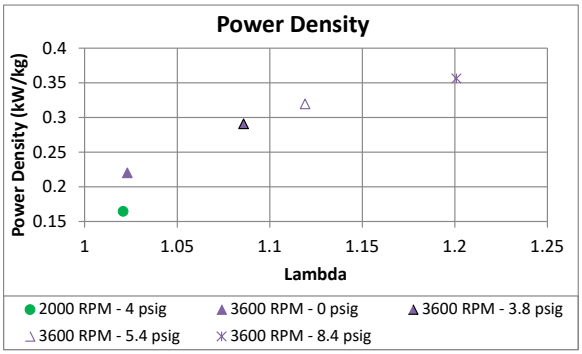

Figure 178: Phase 2 power density

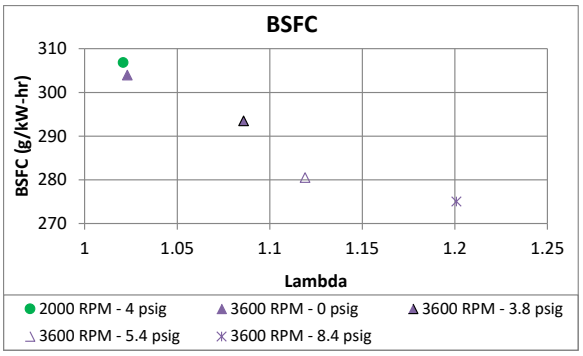

Figure 179: Phase 2 BSFC

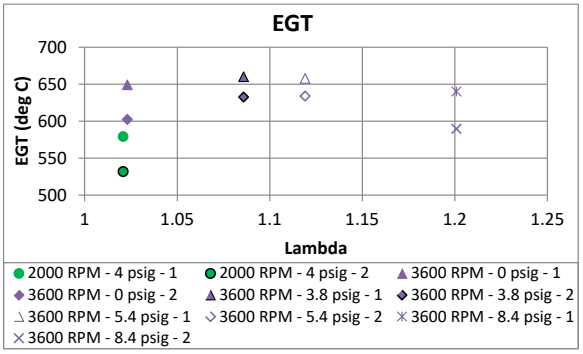

Figure 180: Phase 2 EGT

Fuel Energy Distribution Data

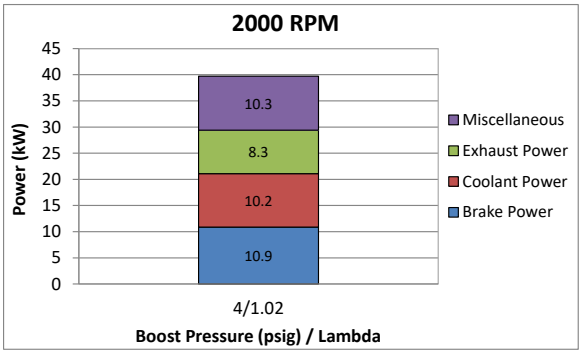

Figure 181: Phase 2 energy distribution @ 2000 RPM

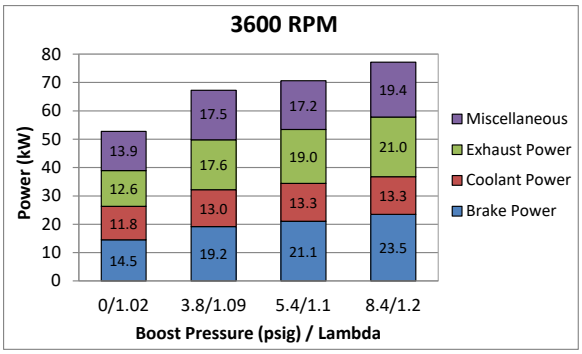

Figure 182: Phase 2 energy distribution @ 3600 RPM

Smoke Data

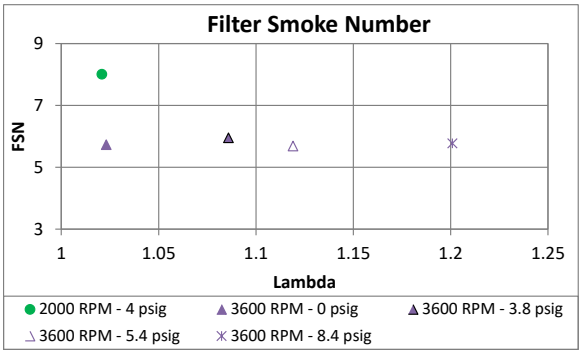

Figure 183: Phase 2 filter smoke number

Combustion Data

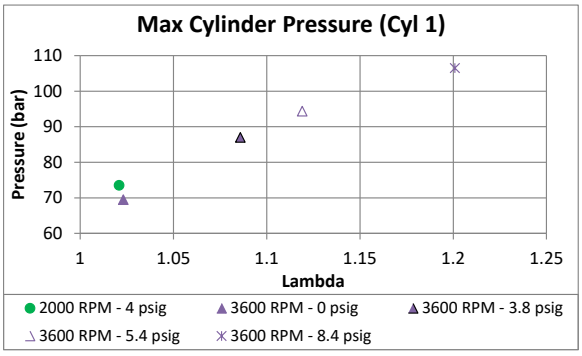

Figure 184: Phase 2 Pmax (cyl 1)

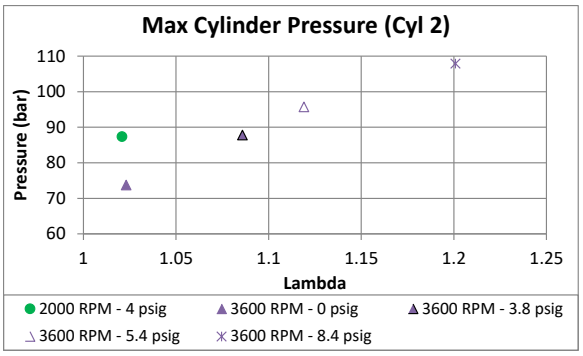

Figure 185: Phase 2 Pmax (cyl 2)

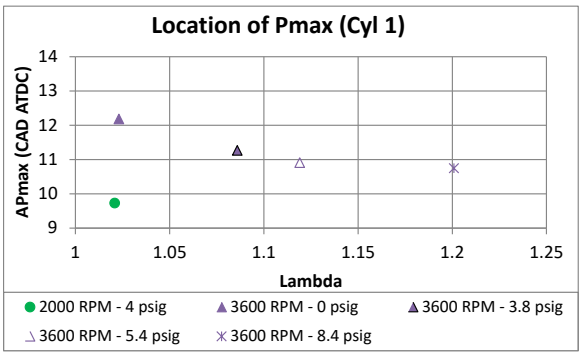

Figure 186: Phase 2 Pmax location (cyl 1)

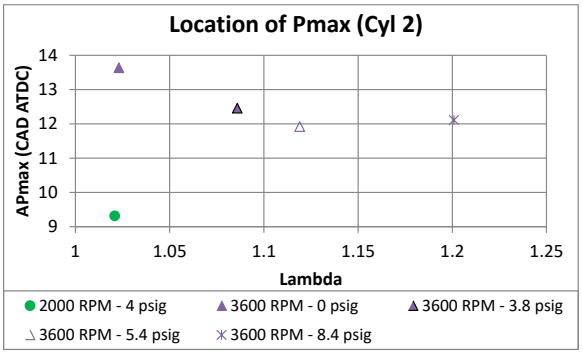

Figure 187: Phase 2 Pmax location (cyl 2)

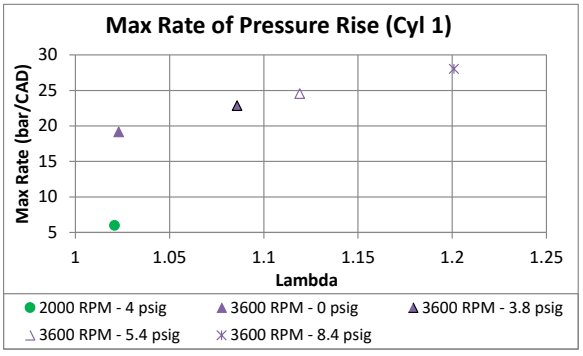

Figure 188: Phase 2 Pmax rise (cyl 1)

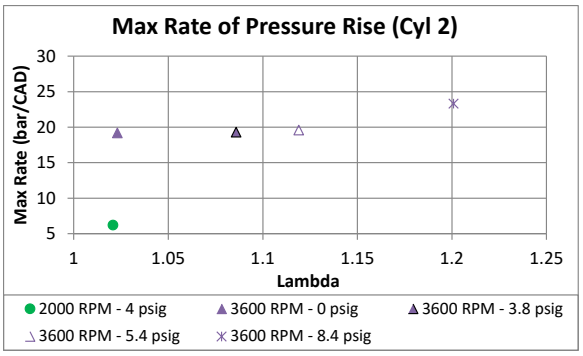

Figure 189: Phase 2 Pmax rise (cyl 2)

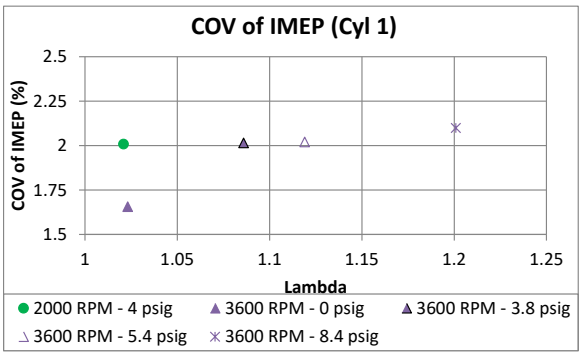

Figure 190: Phase 2 COV of IMEP (cyl 1)

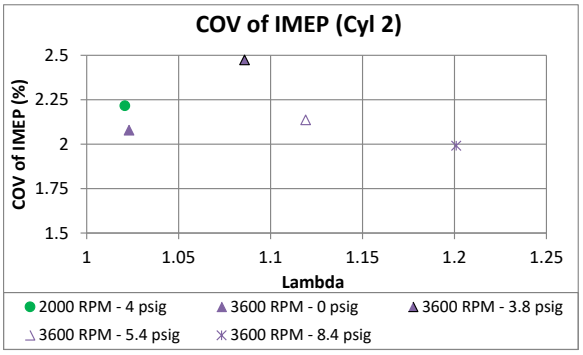

Figure 191: Phase 2 COV of IMEP (cyl 2)

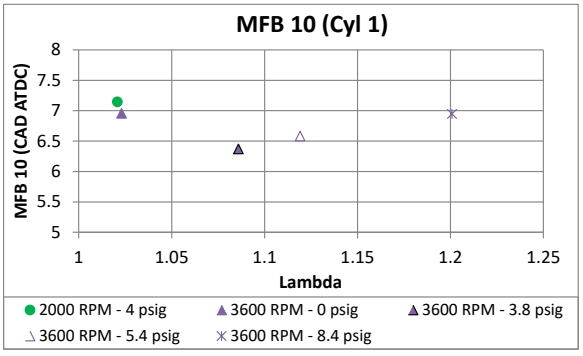

Figure 192: Phase 2 MFB 10 (cyl 1)

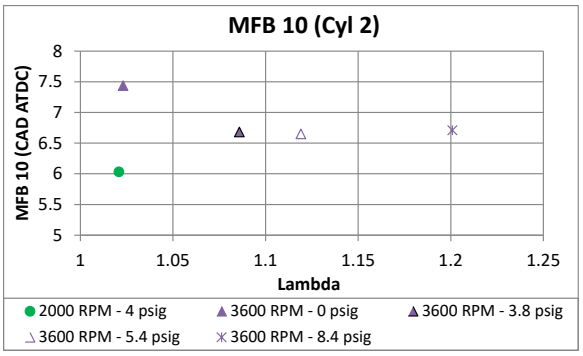

Figure 193: Phase 2 MFB 10 (cyl 2)

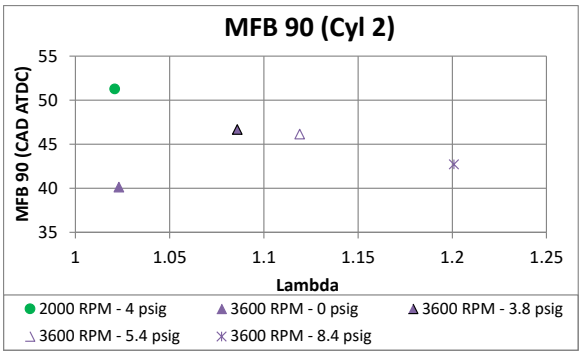

Figure 197: Phase 2 MFB 90 (cyl 2)

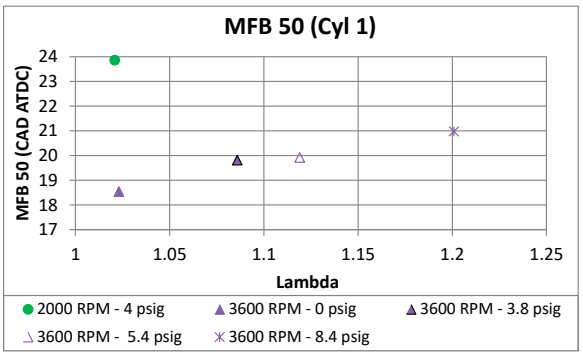

Figure 194: Phase 2 MFB 50 (cyl 1)

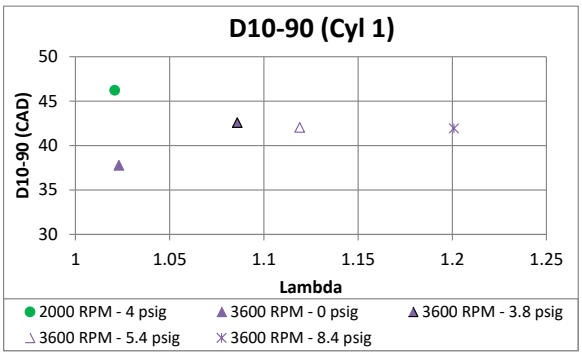

Figure 198: Phase 2 D10-90 (cyl 1)

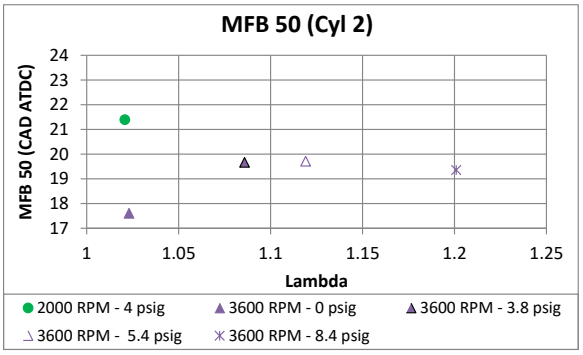

Figure 195: Phase 2 MFB 50 (cyl 2)

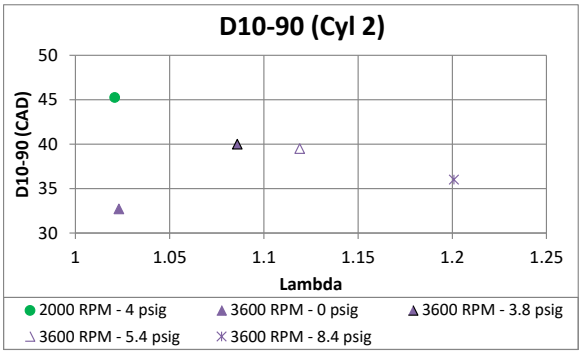

Figure 199: Phase 2 D10-90 (cyl 2)

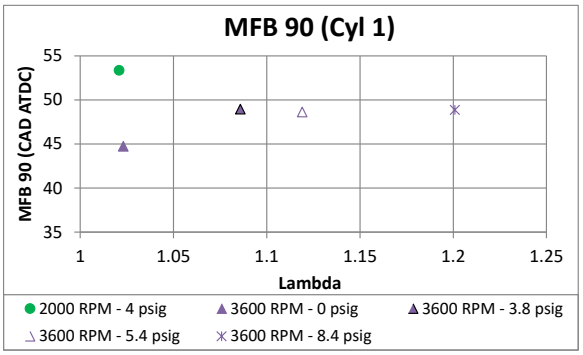

Figure 196: Phase 2 MFB 90 (cyl 1)

Appendix 9: Test Support Drawings

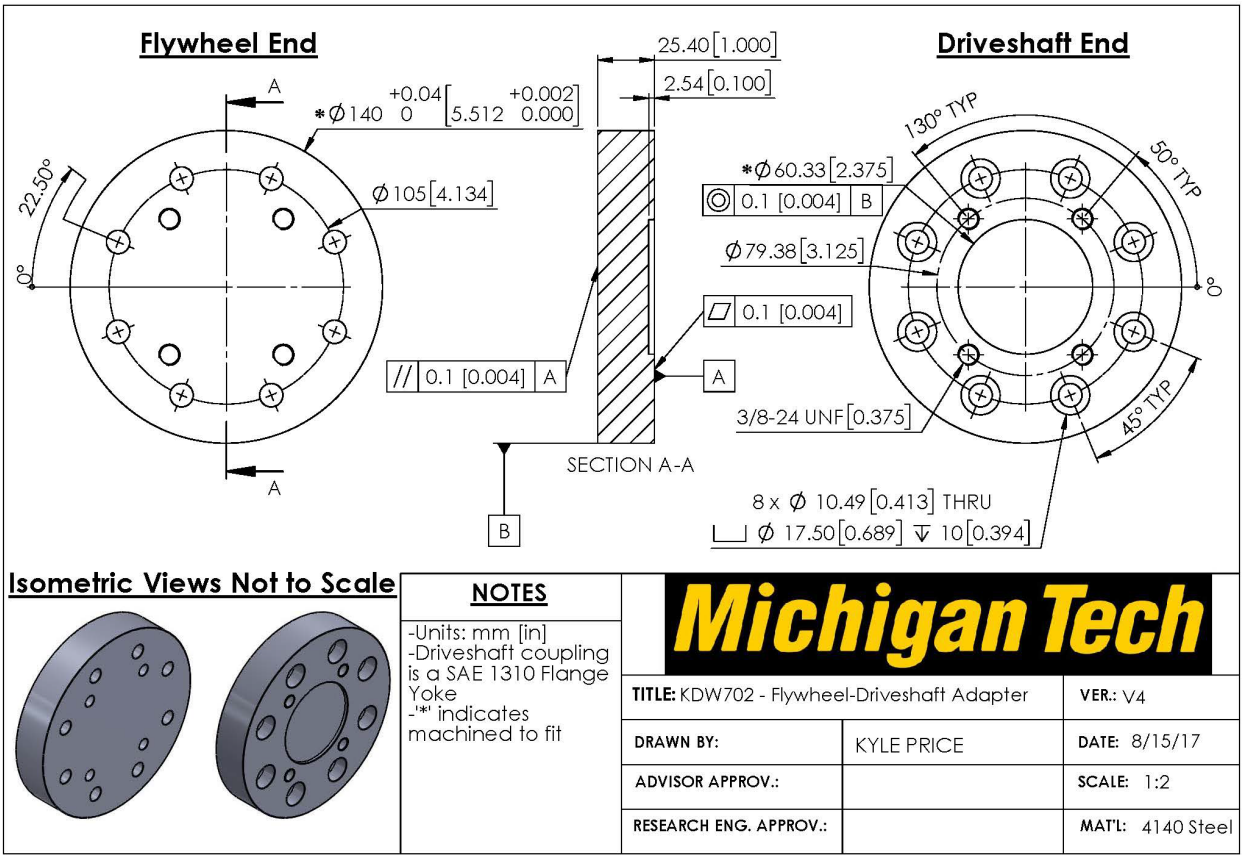

Figure 200: Flywheel adaptor

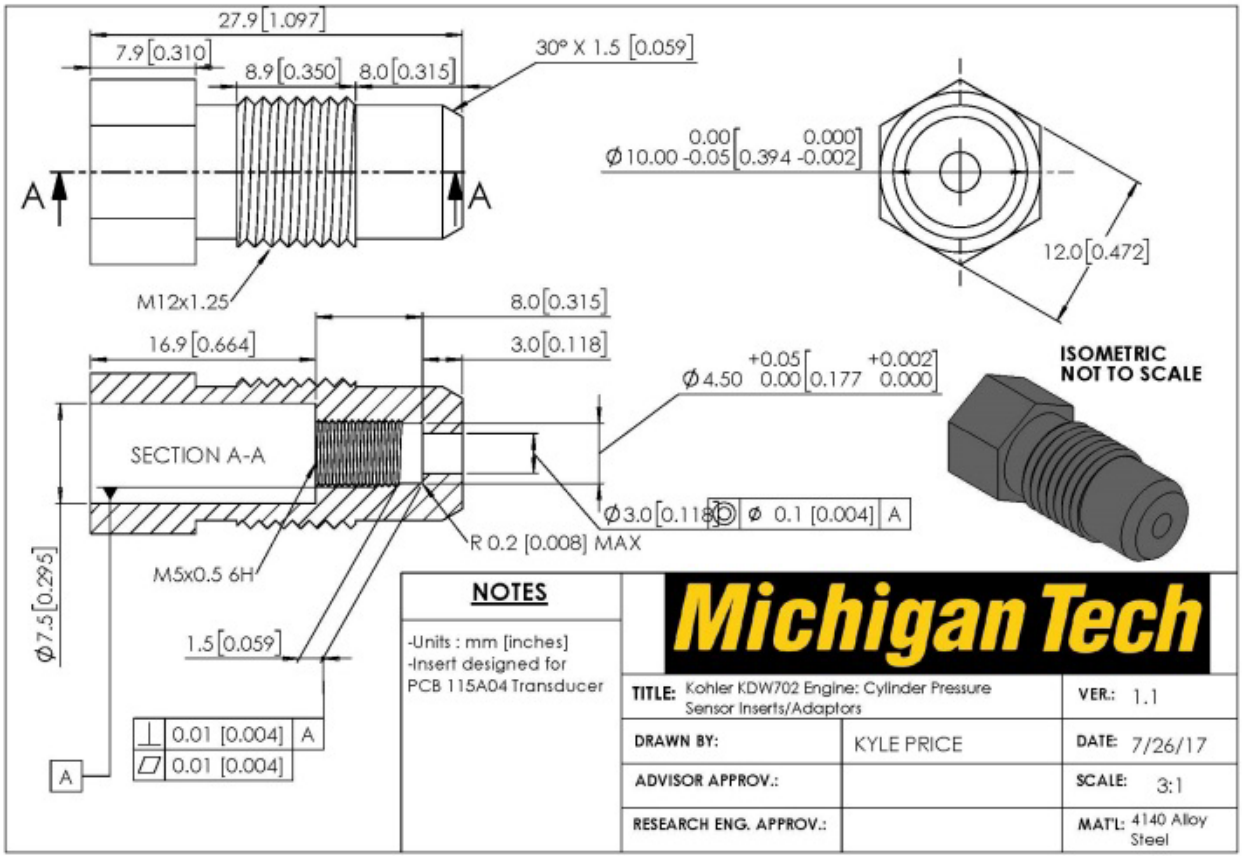

Figure 201: Cylinder pressure transducer adaptor